

Electrodynamics of correlated electron matter

S.V. Dordevic¹, and D.N. Basov²,

¹ Department of Physics, The University of Akron, Akron, OH 44325

² Department of Physics, University of California, San Diego, La Jolla, CA 92093

Received 15 November 2002, revised 30 November 2002, accepted 2 December 2002

Published online 3 December 2002

Key words Strongly correlated electron systems, infrared and optical spectroscopy, extended Drude model.

PACS 78.20.-e, 74.72.-h, 78.30.-j

Infrared spectroscopy has emerged as a premier experimental technique to probe enigmatic effects arising from strong correlations in solids. Here we report on recent advances in this area focusing on common patterns in correlated electron systems including transition metal oxides, intermetallics and organic conductors. All these materials are highly conducting substances but their electrodynamic response is profoundly different from the canonical Drude behavior observed in simple metals. These unconventional properties can be attributed in several cases to the formation of spin and/or charge ordered states, zero temperature phase transitions and strong coupling to bosonic modes.

Copyright line will be provided by the publisher

1 Introduction

Among early seminal successes of quantum mechanics is the advent of the band theory of solids. Within the band theory it became possible to account for fundamental distinctions between the properties of metals and insulators without the need to invoke interactions in the electronic systems. Transition metal oxides including NiO and CuO are notorious examples of the failure of the band theory. The theory prescribes a metallic state in these compounds that are experimentally known to be insulators. Peierls and Mott proposed that this enigma may be related to strong Coulomb interactions between the electrons. This realization, dating back to the late 1930-s instituted the field of correlated electron systems, which to this day remains one of the most vibrant sub-areas of modern condensed matter physics. The last two decades were devoted to the systematic exploration of a diverse variety of materials where complex interplay between charge, spin, lattice and orbital degrees of freedom produces a myriad of interesting effects. These include high- T_c superconductivity, colossal magneto-resistance, spin- and/or charge ordered states, heavy electron fluids and many others. A common denominator between these systems is that the interactions in the electronic systems can no longer be regarded as "weak" as in ordinary metals or semiconductors. While standard theories of metallic conductors are generally inadequate for correlated electron systems it has proven difficult to develop novel theoretical constructs elucidating the complex physics of strong correlations.

Challenges of reaching deep understanding of correlated electron matter prompted development and refinement of experimental techniques most relevant for advancing the experimental picture. A variety of spectroscopic methods traditionally played the crucial role in establishing a description of metals and semiconductors that currently constitutes several chapters in generic texts on condensed matter physics. The last two decades brought dramatic progress in spectroscopies including tunneling, inelastic x-ray scattering, photoemission and infrared/optical spectroscopy. In this article we attempt to discuss some of the recent successes in the studies of the electrodynamic response of correlated electron systems enabled by

e-mail: sasha@physics.uakron.edu

e-mail: dbasov@physics.ucsd.edu

the investigation of the interaction of the electromagnetic radiation in the $\hbar\omega = 1 \text{ meV} - 10 \text{ eV}$ range in several classes of pertinent materials. The key advantage of this particular procedure to study correlations in solids is that it yields information on optical constants in the frequency region that is critical for the understanding of elementary excitations, dynamical characteristics of quasiparticles and collective modes. The optical constants can be modeled using a variety of theoretical approaches. Moreover, in the situations where the theoretical guidance to the data interpretation is insufficient, valuable insights still can be obtained from model independent analysis of the optical constants using a variety of the sum rules. Equally advantageous is the exploration of the power laws in the frequency dependence of the optical constants that in many cases uncovers universalities expected to occur in correlated matter in the proximity to phase transitions.

Regardless of the complexity of a correlated system response, the Drude model of metals is usually employed as a starting point of the examination of the electromagnetic properties. The Drude model establishes a straightforward relationship between electrical and optical properties of metals: a giant leap made by Paul Drude back in 1900 [1, 2]. Indeed, a celebrated Drude expression for the complex optical conductivity $\tilde{\sigma}(\omega) = \sigma_{DC} = (1 - i\omega\tau)^{-1}$ gives a specific prediction for the response of a solid at *all frequencies* based on its DC conductivity σ_{DC} and the relaxation time τ . Even though it is hard to justify the assumptions behind the original derivation, the Drude formula has been remarkably successful in offering simple and intuitive descriptions of mobile carriers in metals and doped semiconductors agreeing well with the experimental facts. As a rule, conducting correlated electron materials reveal significant deviations from the Drude formula. In this article we will examine physical mechanisms underlying unconventional electromagnetic behavior of correlated electron materials.

This article is organized in the following way. We start by discussing experimental procedures used to obtain the optical constants of a solid (Section 2). We then outline the Drude formalism and its modifications in Section 3. Since many correlated electron systems are derived by doping Mott–Hubbard (MH) insulators with holes and/or electrons, we will overview the generic features of the optical conductivity of this class of compounds in Section 4. Doped charges in MH systems often form self-organized spin and/or charge ordered states. It is instructive to explore these states in the context of what is firmly established regarding the properties of more conventional charge- and spin-density wave systems (Section 5). In Section 6 we proceed to unconventional power laws and scaling behavior commonly encountered in correlated electron matter. Section 7 presents a comprehensive analysis of strong coupling effects in high- T_c superconductors with the goal of critically assessing some of the candidate mechanisms of superconductivity. Section 8 focuses on the analysis of the electrodynamics of heavy electron fluids. The analysis of the power laws in the conductivity is continued in Section 9 where we compare and contrast the response of organic and inorganic 1-dimensional conductors. Concluding remarks and outlook appear in Section 10.

2 Experimental observables and measurements techniques

The first step in the quantitative analysis of the electromagnetic response of a solid is a determination of the optical constants of a material out of experimental observables. At frequencies above the microwave region these observables include reflectance $R(\omega)$, transmission $T(\omega)$ and ellipsometric coefficients $\Psi(\omega)$ and $\Delta(\omega)$. As a side note, we point out that the principles of ellipsometry were pioneered by Paul Drude. The real and imaginary parts of complex dielectric function $\tilde{\epsilon}(\omega)$ or the complex conductivity $\tilde{\sigma}(\omega)$ can be inferred through one or several of the following procedures:

1. A combination of reflectance $R(\omega)$ and transmission $T(\omega)$ obtained for transparent materials can be used to extract the dielectric function through analytic expressions. This procedure can be used for film-on-a-substrate systems, as described for example in Ref. [3].
2. Kramers-Kronig analysis of $R(\omega)$ for opaque systems or of $T(\omega)$ for a transparent system.
3. Ellipsometric coefficients for either transparent or opaque material can be used to determine the dielectric function through analytic expressions.

Apart from these protocols based on the intensity measurements, two other techniques are capable of yielding the optical constants directly through the analysis of the phase information:

4. Mach-Zehnder interferometry [4, 5].
5. terahertz time domain spectroscopy [6].

All these methods have their own advantages and shortcomings. For example, (5) is ideally suited for the survey of the temporal evolution of the optical constants under short pulsed photoexcitations [7, 8]. However, the frequency range accessible to this technique is inherently limited to THz and very far-IR. It is worth noting that all these protocols produce the optical constants throughout the entire frequency range where experimental data exist. A notable exception is (2), where both the low- and high-frequency extrapolations required for KK-analysis effectively reduce the interval of reliable data. Nevertheless, KK-analysis of reflectance is the most commonly used technique for the extraction of the optical constants in the current literature. Recently several groups have combined methods (2) and (3) in order to improve the accuracy of IR measurement over a broad frequency range [9, 10]. Experimental advances allow one to carry out reflectance measurements using micro-crystals [11] at temperatures down to hundreds of mK [12, 13] and in high magnetic field [14]. Probably the most powerful attribute of IR/optical spectroscopy is its ability to probe a very broad range of photon energies, spanning several decades from microwave to ultraviolet (Fig. 1). This diagram displays schematically some of the physical phenomena along with the relevant energies. It is apparent that many of these phenomena fall into the part of electromagnetic spectrum which can be and has been probed using IR spectroscopy, as will be discussed below.

3 Understanding electromagnetic response of a solid

In 1900, only 3 years after electron was discovered, P. Drude introduced a simple model for the DC conductivity of metals [1, 2]:

$$\sigma_0 = \frac{ne^2}{m}; \quad (1)$$

where n is the carrier density, m their mass and τ the relaxation time (mean time between collisions). The model has also been generalized for finite frequencies:

$$\sigma(\omega) = \sigma_1(\omega) + i\sigma_2(\omega) = \frac{\sigma_0}{1 - i\omega\tau} = \frac{1}{4} \frac{\omega_p^2}{1 - i\omega\tau}; \quad (2)$$

where, $\omega_p^2 = 4\pi e^2 n / m_b$ is the plasma frequency, n is the carrier density, m_b is the carrier band mass and $1/\tau$ is the scattering rate. The functional form of the model predicts that the real (dissipative) part of the optical conductivity $\sigma_1(\omega)$ is a Lorentzian centered at $\omega=0$. At higher frequencies (i.e. for $\omega \gg 1/\tau$), the model predicts the fall-off $\sigma_1(\omega) \propto \omega^{-2}$. In Section 6 we will report on the detailed analysis of the power law behavior of the optical conductivity of simple and correlated metals.

In addition to this *intra-band* contribution, *inter-band* excitations can also contribute to the optical conductivity and they are usually modeled using finite frequency Lorentzian oscillators:

$$\sigma_{\text{lor}}(\omega) = \frac{1}{4} \frac{\omega_j \omega_{pj}^2}{\omega_j^2 - \omega^2 + i\omega_j\gamma_j}; \quad (3)$$

where ω_j is the frequency of the oscillator, γ_j its width and ω_{pj} the oscillator strength. Other excitations (such as phonons) can also contribute, and they can also be modeled using Eq. 3. A combination of Eqs. 2 and 3 constitutes a so-called *multi-component* description to optical spectra [15].

An obvious problem with the Drude(-Lorentz) models is the assumption of the energy independent scattering rate $1/\tau = \text{const}$. As we will discuss below, in many real materials the scattering rate is known to deviate strongly from this assumption. To circumvent this limitation of constant scattering rate in Eq. 2, J.W. Allen and J.C. Mikkelsen in 1977 introduced a so-called "extended Drude" model [16] in which the scattering rate is allowed to have frequency dependence $1/\tau = \gamma(\omega)$. Causality requires that the quasiparticle effective mass also acquires frequency dependence $m^*(\omega)/m_b$. Both quantities can be obtained from the complex optical conductivity as:

$$\frac{1}{\gamma(\omega)} = \frac{\omega_p^2}{4} < \frac{1}{\gamma(\omega)} = \frac{\omega_p^2}{4} \frac{\gamma_1(\omega)}{\gamma_1^2(\omega) + \gamma_2^2(\omega)}; \quad (4)$$

$$\frac{m^*(\omega)}{m_b} = \frac{\omega_p^2}{4} = \frac{1}{\gamma(\omega)} \frac{1}{\omega} = \frac{\omega_p^2}{4} \frac{\gamma_2(\omega)}{\gamma_1^2(\omega) + \gamma_2^2(\omega)} \frac{1}{\omega}; \quad (5)$$

where the plasma frequency $\omega_p^2 = 4\pi e^2 n/m_b$ is estimated from the integration of $\gamma_1(\omega)$ up to the frequency of the onset of interband absorption. Eqs. 4 and 5 are the basis of a so-called *one-component* approach for the interpretation of optical properties [15].

The optical constants obey various sum rules [15, 17]. The power of these sum rules is that they are based on the most fundamental conservation laws and are therefore model-independent. The most famous and the most frequently used sum rule is the one for the real part of the optical conductivity $\gamma_1(\omega)$:

$$\int_0^\infty \gamma_1(\omega) d\omega = \frac{\omega_p^2}{8} = \frac{ne^2}{2m_0}; \quad (6)$$

and simply expresses the conservation of charge (n is the total number of electrons in the system). Note that in Eq. 6 the integration must be performed up to infinity in order to count all the electrons. From the practical point of view this integration to infinity is not possible. Instead one introduces a so-called effective spectral weight defined as:

$$N_{\text{eff}}(\omega) = \frac{120}{\omega} \int_0^\omega \gamma_1(\omega') d\omega'; \quad (7)$$

which for $\omega \rightarrow \infty$ becomes the sum rule defined by Eq. 6. For finite integration limits the quantity $N_{\text{eff}}(\omega)$ represents the effective number of carriers contributing to optical absorption below the frequency ω . This quantity is particularly useful in studying temperature- and doping-induced changes across phase transitions.

4 Doped transition metal oxides

The last two decades have seen an explosion of interest in doped insulators, in particular doped transition-metal oxides [18]. The interest stems from the fact that some of the physical phenomena that are currently in the focus of condensed matter research, such as high- T_c superconductivity, metal-insulator transitions and colossal magnetoresistance, are realized in doped insulators. Infrared and optical spectroscopy has been one of the most important experimental techniques in the identification of the key signatures of the electronic transport in these novel systems. Fig. 2 shows the in-plane optical conductivity of: $\text{La}_{1-x}\text{Sr}_x\text{TiO}_3$ [19], $\text{La}_{1-x}\text{Sr}_x\text{VO}_3$ [20], $\text{La}_{1-x}\text{Sr}_x\text{MnO}_3$ [21], $\text{La}_{1-x}\text{Sr}_x\text{CoO}_3$ [22], $\text{La}_{2-x}\text{Sr}_x\text{NiO}_4$ [23] and $\text{La}_{2-x}\text{Sr}_x\text{CuO}_4$ [24]. In Fig. 2 these compounds are arranged according to the number of transition metal d -electrons, from Ti with electron configuration $[\text{Ar}]3d^24s^2$, to Cu with configuration $[\text{Ar}]3d^{10}4s$.

Note however that the actual electronic configuration changes as La is being replaced with Sr, as indicated in the figure. All systems shown in Fig. 2 can be doped over a broad range of Sr, driving the compounds through various phase transitions and crossovers. For zero doping ($x = 0$) all systems are antiferromagnetic (AFM) Mott-Hubbard (MH) or charge transfer (CT) insulators [18], as indicated in the figure. They are all characterized by a gap in the density of states, a feature that dominates the response of all undoped parent compounds. As doping x progresses, the gap gradually fills in at the expense of a depression of the spectral weight associated with excitations at higher energy. This process is also accompanied with the development of a zero-energy Drude mode, a clear signature of conducting carriers in the system.

Data presented in Fig. 2 uncover generic characteristics common to diverse classes of doped MH insulators. First, even minute changes of doping lead to radical modification of the optical conductivity extending over the energy range beyond several eV. Similarly, relatively small changes of temperature (100-200 K, i.e. 8.625–17.25 meV) often cause dramatic effects in the complex conductivity of doped MH systems also extending over several eV [18, 25, 26, 27]. These aspects of the Mott transition physics are captured by dynamical mean field theory [28]. The impact of other external stimuli such as electric and magnetic field or photo-doping on the properties of doped MH compounds has not been systematically explored, perhaps with the exception of magnetic fields studies of manganites [29]. Another common feature of doped MH insulators is the deviations of the free carrier response seen in conducting phases from a simple Drude form that will be analyzed in more details in Section 6.

Apart from these universal trends, the dynamical characteristics of mobile charges can be quite distinct in different materials belonging the MH class. These differences are particularly important as far as the behavior of the quasiparticle effective mass m^* in the vicinity of the Mott transition is concerned. The canonical Brinkman and Rice scenario of the Mott transition implies a divergence of m^* at the transition boundary [30]. Imada *et al.* introduced the notion of two distinct types of Mott transitions: i) those driven by band-width and ii) those driven by carrier density [18]. The former type of the transition appears to be realized in $\text{La}_{1-x}\text{Sr}_x\text{TiO}_3$ series [19], where as high- T_c superconductors belong to the latter type [31]. In Fig. 3 we show the effective mass spectra $m^*(\omega)$ (from Eq. 5) for $\text{La}_{1-x}\text{Sr}_x\text{TiO}_3$ [19] and also for high- T_c superconductors $\text{La}_{2-x}\text{Sr}_x\text{CuO}_4$ (LSCO) and $\text{YBa}_2\text{Cu}_3\text{O}_y$ (YBCO) [31]. The top three panels display the doping dependence of the estimated effective mass m^* . In high- T_c superconductors the effective mass is essentially unaffected by the metal-insulator transition. On the other hand in LSCO the mass appears to diverge as one approaches the MH parent compound ($x = 0$). The behavior of other members of La-Sr series (Fig. 2) remains to be explored.

5 Charge and spin ordered states in solids

Many correlated electron materials that are currently at the forefront of condensed matter research reveal tendency toward some form of spin and/or charge ordering at low temperatures. Ordered states have been identified in a variety of materials, including 1D organic systems (TTF-TCNQ and (TMTSF)₂PF₆ [33]), transition metal di- and tri-dichalcogenides (NbSe₂ and NbS₃), transition metal oxides ($\text{La}_{2-x}\text{Sr}_x\text{CuO}_4$ and $\text{La}_{2-x}\text{Sr}_x\text{NiO}_4$), curpate ladders ($\text{Sr}_{14-x}\text{Ca}_x\text{Cu}_{24}\text{O}_4$), etc. In this section we review some of these materials that have recently been studied using infrared spectroscopy.

5.1 Charge density wave and spin density wave systems

Charge density wave (CDW) and spin density wave (SDW) refer to broken symmetry states of metals associated with the periodic spatial variation of the electron or spin density. Signatures of the electromagnetic response of SDW and CDW state include two prominent features: i) a collective mode, typically at very low frequencies and ii) an optical gap [34]. The optical gap is usually described as a Bardeen–Cooper–Schrieffer (BCS) gap in the density of states, with type-II coherence factors. One implication of the latter coherence factors for the optical conductivity $\sigma_1(\omega)$ is that the spectral weight from the intragap region is transferred to frequencies just above the gap, the total spectral weight being conserved, as demanded

by the sum rule Eq. 6. Interesting scaling between the effective mass of the collective mode m and the magnitude of the single particle gap was predicted theoretically by Lee, Rice and Anderson [35]:

$$\frac{m}{m_b} = 1 + \frac{4}{h^2 \omega_{2k_F}^2}; \quad (8)$$

where λ is the electron-phonon coupling constant, ω_{2k_F} is the phonon frequency at $2k_F$ and m_b is the band mass. The scaling relation $m \propto \omega_{2k_F}^{-2}$ was observed experimentally (Fig. 5) to be followed (at least approximately) by a number of conventional CDW systems, such as NbSe_3 , $(\text{NbSe}_4)_2\text{I}$, $(\text{TaSe}_4)_2\text{I}$, etc. [34, 36, 17]. The slope of the line in Fig. 5 is 0.4, somewhat smaller than predicted by Eq. 8. In some CDW materials, especially in 2D and 3D systems, CDW instability does not lead to a complete gap in the density of states. For example, in quasi-2D transition metal dichalcogenides 2H-NbSe_2 and 2H-TaSe_2 , infrared studies have shown that the CDW transition in these systems has very little (if any) effect on the optical properties [37, 38, 39, 40].

The formation of rigid charge density waves is also known to have dramatic implications for optical phonons in solids: new modes are observed corresponding to the lower symmetry of a crystal [34, 41, 42, 43, 44, 45, 46, 47, 48, 49, 50], and also some of the resonances acquire oscillator strengths characteristic of electronic transitions [51]. Previous detailed studies of IR-active phonons provided valuable insights into the charge density wave transition in solids, as well as into the spin-Pierls physics [52, 53, 54].

A canonical example of a spin density wave system is metallic chromium Cr. Its IR spectrum has been reported by Barker *et al.* [55] and more recently by Basov *et al.* [56]. Above $T_{\text{SDW}} = 312 \text{ K}$ the IR spectrum is typical of metals, with a well defined Drude-like peak. A more detailed analysis of the conductivity uncovered the frequency dependent scattering rate $1/\tau(\omega)$ following ω^2 behavior (Fig. 4). The ω^2 power law is expected for canonical Fermi liquids (see Section 6 below). As temperature falls below T_{SDW} a gap opens over some parts of the Fermi surface as a consequence of SDW ordering. Gap opening manifests itself in the IR spectra: the Drude mode narrows and the low energy spectral weight is suppressed, resulting in a finite frequency maximum in $1/\tau(\omega)$ (Fig. 4). The optical scattering rate in the SDW state acquires a non-trivial dependence: it is suppressed below $\omega < 500 \text{ cm}^{-1}$ and then overshoots the high-T curve. These results uncover profound and non-intuitive consequences of an opening of a partial (incomplete) gap in the density of states (DOS) of a metallic system. Even though the density of states at E_F is reduced, the DC and low- ω AC conductivity are enhanced. That is because the reduction of DOS is accompanied with the reduction of the low- ω scattering rate. The two effects compete, and in some cases like Cr, the latter overpowers the former, leading to "more metallic" behavior in the gaped state. As a side remark we note that the "area conservation" in the $1/\tau(\omega)$ data taken above and below the SDW transition [56]. This effect is a property of the BCS density of states [57, 58]. The behavior is relevant for the understanding of the pseudogap in oxides and other correlated electron systems. Basov *et al.* [56] argued that in hole-doped cuprates the opening of a pseudogap does not conserve the area under $1/\tau(\omega)$ spectra. This finding is in conflict with the interpretation of the pseudogap in terms of superconducting and/or charge/spin density wave gap which all preserve the area in $1/\tau(\omega)$ data.

5.2 Charge and spin ordering in strongly correlated oxides

An unconventional form of spin and charge ordering has been theoretically proposed and experimentally observed in transition metal oxides, particularly nickelates and cuprates [59]. In these systems strong electron-electron correlations lead to self-organization of charge carriers into 1D objects referred to as stripes. The role of stripes in high- T_c superconductivity of cuprates is a highly debated issue [59]. Unmistakable evidence for charge and spin stripes is found for Nd-doped $\text{La}_{2-x}\text{Sr}_x\text{CuO}_4$ system. A static stripe order is likely to induce an energy gap discussed in the previous section. However, such a gap is not resolved in IR measurements [60, 61]. Nd-free $\text{La}_{2-x}\text{Sr}_x\text{CuO}_4$ crystals reveal evidence for spin stripes based on neutron scattering data whereas the corresponding charge ordering peaks are not apparent [62].

Infrared studies carried out by Dumm *et al.* [63] uncovered significant anisotropy of the optical conductivity with the enhancement of $\sigma_1(\omega)$ in far-IR by as much as 50% along and the direction of the spin stripes [63]. Padilla *et al.* searched for the evidence of phonon zone-folding effects in $\text{La}_{2-x}\text{Sr}_x\text{CuO}_4$ crystals showing the anisotropy of the optical conductivity attributable to spin stripes [31]. No evidence for additional phonon peaks beyond those predicted by group theory has been found. This latter result points to a departure of the spin ordered state in cuprates from a conventional stripe picture.

Some form of SDW state has been inferred from the analysis of IR data for electron-doped cuprates, such as $\text{Pr}_{2-x}\text{Ce}_x\text{CuO}_4$ (PCCO) [64] and $\text{Nd}_{2-x}\text{Ce}_x\text{CuO}_4$ (NCCO) [65]. Zimmers *et al.* have measured a series of PCCO samples with $x=0.11$ (non-superconducting), 0.13 (underdoped $T_c=15$ K), 0.15 (optimally doped $T_c=21$ K) and 0.17 (overdoped $T_c=15$ K). In all but the overdoped sample they observed a gap-like feature in the low-temperature spectra. Their theoretical calculations based on tight-binding band structure augmented with an optical gap of magnitude 0.25 eV were able to reproduce the most important features of $\sigma_1(\omega)$ spectra. This optical gap was claimed to be a density wave gap induced by commensurate (π, π) magnetic order. Interestingly the optical gap was identified even in the optimally doped sample ($x=0.15$), for which no magnetic order has been observed in neutron scattering experiments. Similarly Onose *et al.* claimed SDW in NCCO samples [65]. Wang *et al.* [66] reported analysis of the in-plane optical data for a series of NCCO crystals in terms of the energy dependent scattering rate. In underdoped materials they observe a characteristic non-monotonic form of $1/\tau(\omega)$ consistent with the BCS form of the density of states. These findings support the SDW interpretation of the IR results for electron doped compounds.

Chakravarty *et al.* [67] proposed that the totality of transport and spectroscopic data for hole-doped cuprates is consistent with a new form of long-range density wave, with d-wave symmetry of its order parameter (DDW). It has been theoretically predicted that signatures of this peculiar order could be observed in the infrared spectra. Valenzuela *et al.* [68] and Gerami and Nayak [69] have carried out numerical analysis of possible effects in the optical conductivity and claimed that some of these effects might have already been seen. In particular the transfer of spectral weight in $\sigma_1(\omega)$ with opening of pseudogap is consistent with the predictions of the DDW model.

Recently signatures of density waves have also been identified in cuprate ladder compounds. Osafune *et al.* [70] investigated infrared response of the two-leg ladder system $\text{Sr}_{14-x}\text{Ca}_x\text{Cu}_{24}\text{O}_4$ for two doping levels $x=8$ and 11. In both cases c-axis conductivity spectra (along the ladders) at room temperature revealed a monotonic frequency dependence. However as temperature was lowered the optical conductivity along c-axis $\sigma_c(\omega)$ of both compounds developed a finite frequency peak in the far-IR part of the spectrum. Osafune *et al.* argued that the peak is a collective mode of a pinned CDW, as opposed to carrier localization that was used to explain similar finite frequency modes in disordered cuprate superconductors [71]. Based on the spectral weight of the peak, Osafune *et al.* estimated the effective mass to be 100 free-electron masses for the $x=11$ sample, and 200 free-electron masses for the $x=8$ sample. These large values signal a collective nature of the excitations. Vuletic *et al.* have also studied the ladder systems $\text{Sr}_{14-x}\text{Ca}_x\text{Cu}_{24}\text{O}_4$ with $x=0, 3$, and 9, but inferred somewhat smaller values of the effective masses $20 < m^* < 50$ [72].

Density wave states have been claimed in a number of oxide materials which do not show static long range order in diffraction experiments (X-ray and/or neutron scattering). For example, the optical conductivity of a layered ruthenium oxide BaRuO_3 displays an opening of a pseudogap at low temperatures and characteristic blue shift of the the spectral weight [73]. This was interpreted in terms of a fluctuating CDW order in the system. Similar transfer of spectral weight was observed in the IR spectra of ferromagnetic BaInO_3 [74]. In this quasi-1D transition metal oxide, the ferromagnetic ordering at $T_c=175$ K was accompanied by CDW formation. Moreover, Cao *et al.* argued that the ordered magnetism was *driven* by CDW formation or partial gapping of Fermi surface.

Recently discovered Na_xCoO_2 compounds attracted a lot of attention because of the superconductivity in hydrated samples [75]. Sodium contents x can be changed from 0 to 1, which drives the system to various ground states. For $x > 3/4$ Na_xCoO_2 is in a spin ordered phase, near $x=2/3$ it is a Curie-Weiss metal, a charge-insulator for $x = 1/2$, and a paramagnetic metal for $x = 1/3$. Infrared spectroscopy has been performed on samples with different doping levels [76, 77, 78, 79, 80]. Samples with Na doping $x=0.5$

[79] and 0.82 [80] revealed tendency toward charge ordering. On the other hand infrared spectra of the sample with $x=0.7$ doping indicated proximity to a spin-density-wave metallic phase [78].

We conclude this section with an interesting observation that the scaling between the optical gap and effective mass (Eq. 8) predicted for conventional CDW systems, also seems to work well for cuprate ladders $\text{Sr}_{1-x}\text{Ca}_x\text{Cu}_2\text{O}_4$ (Fig. 5). The only exception is the sample with $x=9$, for which a very small value for the gap was inferred from the data [72]. Osafune *et al.* inferred a much larger value of the gap for similar doping levels ($x=8$ and 11) [70]. The reason for this discrepancy is the interpretation of the far-IR feature, which was interpreted as a pinned CDW mode by Osafune *et al.* and as the onset of a CDW gap by Vuletic *et al.*. Interestingly, the scaling (Eq. 8) is also followed by metallic chromium Cr , a canonical SDW system. On the other hand electron-doped cuprates, such as $\text{Pr}_{2-x}\text{Ce}_x\text{CuO}_4$ (PCCO) and $\text{Nd}_{2-x}\text{Ce}_x\text{CuO}_4$ (NCCO), do not seem to follow the scaling.

6 Unconventional power laws and quantum criticality

The canonical Drude expression Eq. 2 offers an accurate account of the conductivity for a system charges with short-ranged interactions and predicts a power-law behavior $\sigma_1(\omega) \propto \omega^{-2}$ at $\omega \rightarrow 0$. A salient feature of essentially every system belonging to the class of "strongly correlated materials" is a departure from the ω^{-2} response. In many systems the conductivity follows the power law form $\sigma_1(\omega) \propto \omega^{-\alpha}$ with $\alpha < 2$. In cuprate high- T_c superconductors near optimal doping, $\sigma_1(\omega)$ reveals the power law conductivity with $\alpha \approx 0.65-0.7$ [81, 82, 83] as exemplified in Fig. 6. The ruthenate SrRuO_3 ($\sigma_1(\omega)$) shows power law behavior with $\alpha \approx 0.5$ [84, 85, 86]. In this Section we will present a survey of unconventional (non-quadratic) power laws in the conductivity of several classes of correlated electron system and will discuss different scenarios proposed to account for this enigmatic behavior.

Power law scaling has been explored in great details in SrRuO_3 Dodge *et al.* [85] using a combination of terahertz time domain spectroscopy by infrared reflectivity and transmission. A broad spectral coverage has allowed the authors to examine scaling laws over nearly three decades in frequency ($6-2400 \text{ cm}^{-1}$). These authors found the power law behavior with $\alpha \approx 0.4$ in the low temperature conductivity. An extended frequency range in the data set has uncovered unexpected aspects of a connection between THz/IR conductivity and the DC transport. Spectra in Fig. 7 clearly show that the divergence of $\sigma_1(\omega)$ at low frequencies is avoided on the frequency scale set by the scattering rate Γ , thus enforcing $\sigma_1(\omega \rightarrow 0) \propto \Gamma$. This observation is important since it challenges the ubiquitous practice of inferring relaxation times from dc transport via $\tau_{dc} \propto \sigma_{dc}$ relation. Indeed, the latter relation becomes erroneous if the conductivity follows the power law deviating from the simple Drude result Eq. 1. Specifically, in the case of SrRuO_3 the resistivity is linear with temperature between 25 K and 120 K, implying a quadratic temperature dependence of the relaxation rate (inset of Fig. 7). A similar non-linear relationship between the dc data and the scattering rate has been observed in another itinerant ferromagnet, MnSi , by Mena *et al.* [87].

It is commonly asserted that the power law behavior of the conductivity with $\alpha \neq 2$ signals the breakdown of the Fermi liquid description of transport in correlated electron systems. It is worth pointing out that in this context $\sigma_1(\omega) \propto \omega^{-2}$ behavior is a consequence of frequency independent scattering rate in the simple Drude formula. However, the canonical Fermi liquid theory predicts the scattering rate that varies quadratically both as a function of frequency and temperature:

$$\frac{1}{\sigma_1(\omega; T)} = \frac{1}{\sigma_0} + a(\hbar\omega)^2 + b(k_B T)^2 \quad (9)$$

with $b/a = \omega^2$. This latter behavior is observed, for example, in the elemental metal Cr [56] (see Fig. 4). It is easy to verify that Eq. 9 does not modify the ω^{-2} character of the real part of the conductivity. However, the imaginary part of the conductivity of a FL metal and a Drude metal show very different power laws. In Table 1 we display results of both analytical and numerical calculations of optical constants $\sigma_1(\omega)$ and $\sigma_2(\omega) = \frac{1}{2} \frac{d\sigma_1(\omega)}{d\omega}$ for several different models. For the models of Drude (Eq. 2) and Ioffe and

Table 1 The power laws of the optical constants $\epsilon_1(\omega)$ and $j_1(\omega)/j_2(\omega) = \frac{\epsilon_1(\omega)}{\epsilon_2(\omega)}$. For Drude, and Ioffe–Millis’ models analytical calculations were employed, whereas for the Marginal Fermi Liquid and Landau Fermi Liquid we used simple numerical calculations.

	$\epsilon_1(\omega)$	$j_1(\omega)/j_2(\omega)$
Drude	ω^{-2}	ω^{-1}
Landau FL	ω^{-2}	ω^{-2}
Marginal FL	$\omega^{-0.45}$	$\omega^{-0.725}$
Ioffe–Millis	$\omega^{-0.5}$	$\omega^{-0.5}$
Generalized I-M	ω^{-1}	ω^{-1}

Millis [88] ($\epsilon_1(\omega) = \epsilon_0 \frac{\omega_p^2}{\omega^2 + \gamma^2}$ and $j_1(\omega) = \frac{\gamma}{\omega^2 + \gamma^2}$ respectively) we derived simple analytical expressions. For Landau (Eq. 9) and Marginal Fermi Liquid ($\epsilon_1 = \epsilon_2 = \epsilon_0$) we used KK analysis to obtain the imaginary part.

We now discuss several theoretical proposals to account for the unusual power laws both within the Fermi liquid theory and also using non-Fermi Liquid approaches. In order to account for the non-Drude power law behavior of the conductivity within the FL approaches one is forced to invoke rather anomalous scattering mechanisms. One of the earliest accounts is the so-called Marginal Fermi Liquid (MFL) theory postulating scattering of quasiparticles from a bosonic spectrum that is flat over frequency scale from $T < \omega < \omega_c$ where ω_c is a cut-off frequency [89]. The MFL theory assumes the following form of the electronic self-energy $\Sigma(\omega) = -i \ln(x/\omega_c) + i x$ where $x = m a x(\omega; T)$. The model is in fair agreement with experiments on high- T_c cuprates especially at not so low temperatures [90]. Alternatively, power law behavior of the optical constants has been explored assuming strong momentum dependence of the quasiparticle lifetime along the Fermi surface [91, 92, 93, 88]. Interestingly, this momentum dependence originally inferred from the analysis of transport and infrared data in Refs. [91, 92, 88] was later confirmed by direct measurements using angle resolved photoemission spectroscopy (ARPES) [94]. Specifically, the “cold spots” model of Ioffe and Millis not only predicts the power law behavior of the conductivity with $\omega^{-0.5}$ for the in-plane conductivity, but also offers an account of the gross features of the interplane transport [88, 95]. The momentum dependence of the quasiparticle lifetime is a natural feature of the spin fluctuation model of Chubukov *et al.* [96]. The power law behavior of the conductivity within this model has been analyzed in Ref. [97] in the context of crossover from FL to non-FL behavior above a characteristic energy ω_{sf} . Relevance of spin fluctuations to the power law behavior of the optical data with $\omega^{-0.65}$ also emerges out of numerical results obtained within the t-J model by Zemljic and Prelovsek [98].

Unlike the (generalized) Fermi liquid models, the non-FL approaches propose that current carrying objects are not simple electrons but instead may involve spinons and holons [99] or phase fluctuations of the superconducting order parameter [100]. Both of these approaches predict the power law behavior of the optical constants. Ioffe and Kotliar considered optical conductivity of spin-charge separated systems and derived the form $\epsilon_1(\omega) / \epsilon_2(\omega) = (T + \omega)^{-1}$ [101, 88]. Depending whether spinons or holons dominate the transport the magnitude of ϵ_1 is predicted to be 4/3 or 3/2. Anderson proposed that a non-Drude power law is a natural consequence of the Luttinger-liquid theory with spin-charge separation [102].

The analysis of the power law behavior and of the frequency/temperature scaling of the optical constants is interesting in the context of quantum phase transitions occurring at $T \rightarrow 0$ to the electronic properties of correlated electron systems. In the vicinity of such a transition a response of a system to external stimuli is expected to follow universal trends defined by the quantum mechanical nature of fluctuations [103, 104, 105]. Van der Marel observed $\omega = T$ scaling in the response of optimally doped high- T_c superconductor $\text{Bi}_2\text{Sr}_2\text{Ca}_{0.92}\text{Y}_{0.08}\text{Cu}_2\text{O}_8$ [83]. Both under- and over-doped counterparts of this system did not reveal a similar scaling. This result is indicative of the association of the quantum critical with optimized transition temperature in high- T_c materials. Lee *et al.* reported an observation of $\omega = T$ scaling

of the optical conductivity in CaRuO_3 system [86]. These authors attributed the quantum critical point to a zero temperature transition between ferromagnetic and paramagnetic phases.

We conclude this section by pointing out another class of materials with "non-FL" electrodynamics. Degiorgi *et al.* investigated a variety of heavy-electron systems which they also qualified as "non-Fermi-Liquid" [106, 107]. These materials (such as: $\text{U}_{0.2}\text{Y}_{0.8}\text{Pd}_3$, $\text{UCu}_{3.5}\text{Pd}_{1.5}$, $\text{U}_{1-x}\text{Th}_x\text{Pd}_2\text{Al}_3$, and others) typically show a non-monotonic form of the conductivity dominated by a stark resonance at mid-IR frequencies. This non-monotonic form of $\sigma_1(\omega)$ distinguishes U-based non-FL compounds from doped MH insulators discussed in this sections. The non-FL behaviour in these systems is usually explained in terms of multichannel Kondo models, models based on proximity to quantum critical points, or models based on a disorder [108].

7 Strong coupling effects in cuprates

It is widely believed that charge carries in cuprates are strongly coupled to bosonic excitations. Signatures of strong coupling have been evidenced by a number of experimental techniques such as IR, ARPES and tunneling. However the nature of bosonic excitations to which carriers are coupled is currently one of the most debated subject in the field. Both phonons [109, 110, 111, 112] and spin fluctuations [113, 114, 115] are currently considered as possible candidates. At issue is whether or not the magnetic mode is capable of having a serious impact on the electronic self-energy, in view of the small intensity of the resonance [116, 117, 118].

In order to discriminate between the candidate mechanisms it is desirable to learn as many details as possible regarding the Eliashberg spectral function $^2F(\omega)$ quantifying strong coupling effects. This is a challenging task. The key complication is that physical processes unrelated to strong coupling can in principle mimic spectral signatures of quasiparticles coupled to bosonic modes. Specifically, the energy gap or pseudogap is known to produce a characteristic threshold structure in the $1=\sigma_1(\omega)$ data [119, 120, 121] that makes it difficult to infer $^2F(\omega)$ from the raw data. It is therefore imperative to treat consistently the two effects: (pseudo)gaps in the density of states and the coupling of charge carriers to some bosonic mode [120]. We will discuss a new approach to this problem recently proposed by Dordevic *et al.* [122] after giving the necessary background.

In 1971 P. Allen studied signatures of strong electron-phonon coupling in the infrared spectra of metals and derived the following formula for the optical scattering rate at $T=0$ K [123]:

$$\frac{1}{\sigma_1(\omega)} = \frac{2}{\omega} \int_0^{\omega} d\omega' \left(\frac{\omega'}{\omega} \right)^2 F(\omega'); \quad (10)$$

This $T=0$ results has been generalized to finite temperatures by Millis *et al.* [124] and Shulga *et al.* [125]:

$$\frac{1}{\sigma_1(\omega; T)} = \frac{2}{\omega} \int_0^{\omega} d\omega' \left(\frac{\omega'}{\omega} \right)^2 F(\omega'; T) \frac{h}{2T} \coth \frac{h}{2T} \left(\frac{\omega'}{\omega} + \frac{h}{2T} \right) \coth \frac{h}{2T} \left(\frac{\omega'}{\omega} - \frac{h}{2T} \right) \coth \frac{h}{2T} \left(\frac{\omega'}{\omega} \right); \quad (11)$$

which in the limit $T \rightarrow 0$ K reduces to Allen's result Eq. (10).

The integral form of Eqs. 10 and 11 implies that the task of extraction of $^2F(\omega)$ from experimental data is non-straightforward and calls for the development of suitable inversion protocols. To extract the electron-phonon spectral function in a conventional superconductor lead Pb Marsiglio *et al.* employed the differential form of Eq. 10 [126]:

$$W(\omega) = \frac{1}{2} \frac{d^2}{d\omega^2} \left(\frac{1}{\sigma_1(\omega)} \right); \quad (12)$$

where $W(\omega)$ is a function closely related to $^2F(\omega)$ [126]. The spectral function obtained with Eq. 12 was in good agreement with $^2F(\omega)$ inferred from tunneling measurements [126]. Eq. 12 requires taking the second derivative of experimental data, which introduces significant numerical difficulties. The experimental data must be smoothed before derivatives can be taken. In order to avoid the differentiation problems Tu *et al.* [127] and Wang *et al.* [128] fitted the optical spectra (reflectance or scattering rate) with polynomials and then used Eq. 12 to calculate $^2F(\omega)$. Casek *et al.* [129] have also used Eq. 12 to generate the electron-boson spectral function from the model conductivity spectra, calculated within the spin-fermion model. Hwang *et al.* have modeled the scattering rate spectra $1/\tau(\omega)$ with the formula which includes a non-constant density of states around the Fermi level [130, 131].

Carbotte, Schachinger and Basov have also applied Eq. 12 to extract the electron-boson spectral function in the high- T_c cuprates [114]. Fig. 8 displays an example of these calculations for optimally doped $\text{YBa}_2\text{Cu}_3\text{O}_{6.95}$. The electron-boson spectral function $^2F(\omega)$ extracted this way shows a characteristic shape, dominated by a strong peak, followed by a negative dip. Carbotte *et al.* interpreted the peak as due to coupling of charge carriers to neutron "resonance" [114]. Previously, the idea of quasiparticles coupling to a neutron mode had been proposed by Norman and Ding [132] and Munzar [115].

A cursory examination of Fig. 8 uncovers one obvious problem of the second-derivative protocol: negative values in $^2F(\omega)$ are unphysical. This artifact of the analysis stems from either the numerical instabilities or the application of Eqs. 10 or 12 to systems with a (pseudo)gap in the density of states [133]. In his celebrated 1971 article [123] P. Allen also derived the formula for the scattering rate in the superconducting state at $T=0$ K, i.e. in the presence of a gap in the density of states:

$$\frac{1}{\tau(\omega)} = \frac{2}{\omega} \int_0^{\omega} d\omega' \left(\frac{1}{\omega'} - \frac{1}{\omega - \omega'} \right) ^2F(\omega') E(x) \frac{h^S}{1 - \frac{4\omega'^2}{(\omega - \omega')^2}} \quad (13)$$

where ω is the (momentum-independent) energy gap and $E(x)$ is the complete elliptic integral of the second kind. For $\omega=0$ Eq. 13 reduces to Eq. 10.

The extraction of $^2F(\omega)$ from Eq. 13 is non-trivial, as the corresponding differential expression does not exist. The integral equation must be solved (inverted) directly. Dordevic *et al.* have used a so-called singular value decomposition (SVD) method to calculate the spectral function from Eq. 13 [122]. Fig. 9 displays inversion calculations for optimally doped YBCO (the same as in Fig. 8) with several different gap values

. As the gap value increases, the negative dip in the $^2F(\omega)$ spectra diminishes and for 150 cm^{-1} it is almost completely absent. An obvious problem with these calculations is that they assume: i) s-wave gap and ii) $T=0$ limit. Neither of these assumptions are valid for cuprates. However even with these inadequacies Eq. 13 is useful, because it allows one to treat both effects (coupling to bosonic mode and gap in the density of states) on equal footing. Carbotte and Schachinger have developed similar analysis protocol which takes into account d-wave symmetry of the order parameter [134].

The extraction of the spectral function $^2F(\omega)$ from $1/\tau(\omega)$ spectra can be complemented with the analogous inversion procedure applied to the effective mass spectra $m^*(\omega)/m_b$ (Eq. 5). The corresponding formula derived by Chubukov [135]:

$$\frac{m^*(\omega)}{m_0} = 1 + 2 \int_0^{\omega} d\omega' ^2F(\omega') \frac{h_1}{\omega'} \log \frac{\omega + \omega'}{\omega - \omega'} + \frac{1}{\omega'^2} \log \frac{2}{2 - \frac{\omega'^2}{\omega - \omega'}} \quad (14)$$

is mathematically of the same type as Eqs. 11 and 13 (the so-called Fredholm integral equation of the first kind). Figure 10 displays results of numerical calculations of the spectral function of underdoped $\text{YBa}_2\text{Cu}_3\text{O}_{6.65}$. The top panel is $^2F(\omega)$ obtained from the scattering rate $1/\tau(\omega)$ (using Eq. 11) and the bottom panel from effective mass $m^*(\omega)/m_b$ (using Eq. 14). Both inversions produce similar results, in particular a strong peak, followed by a negative dip.

The inversion protocol based on the SVD algorithm can also be applied to ARPES data [122]. The procedure is based on the analysis of the real part of the electron self-energy ($\Sigma_1(\omega)$), which is experimentally accessible through ARPES. One must keep in mind that the spectral functions probed in The two experiments are not the same: ARPES probes the equilibrium $\chi^2_F(\omega)$ which is a single-particle property, whereas IR measures transport $\chi^2_{tr}(\omega)$, a two-particle property. Moreover ARPES is a momentum resolving technique, whereas IR averages over the Fermi surface. In the latter case, the effect of a d-wave energy gap must be taken into account, which effectively shifts the peak up to higher energies. In the ARPES case the energy gap (either superconducting or pseudogap) should not play a role, if the data is taken along nodal direction.

The spectral functions obtained from ARPES have some similarities, but also some important differences compared with IR. The resolution of ARPES data is presently poorer than IR, which implies that even fewer features could be resolved in the spectral function. The ARPES $\chi^2_F(\omega)$ also has a strong peak, but unlike IR the negative dip seems to be absent. Also the high-energy contribution is not identified in the ARPES results. The position of the main peak is particularly interesting. The most direct comparison can be made for optimally doped $\text{Bi}_2\text{Sr}_2\text{CaCu}_2\text{O}_{8+}$ (Bi2212), for which both high quality IR and ARPES data exist. The analysis has shown that the peaks actually occur at roughly the same frequency in both ARPES and IR spectral functions. This result is surprising and unexpected, as the main peak in the IR $\chi^2_F(\omega)$ is supposed to occur at higher frequencies (shifted by the gap). Hwang *et al.* have made a similar comparison between the electron self-energy obtained from IR and ARPES for several different doping levels [136]. High quality ARPES and IR data for the cuprate families of LSCO and NCCO have recently become available [31, 64, 112, 137] and future analysis will reveal if the behavior observed in Bi2212 is universal.

8 Heavy fermion systems

Heavy fermion metals are intermetallic compounds which contain certain rare-earth elements, such as U, Ce, or Yb. They are characterized by large enhancements of their quasiparticle effective mass m^* . The electronic properties of HF metals are in accord with a scenario based on hybridization of localized f electrons and delocalized s , p or d electrons [28, 138, 139, 140, 141, 142]. At high temperatures the hybridization is negligible and the properties are described by two independent sets of electrons. However, at low temperatures hybridization leads to mixing of conduction and f -electrons and opening of a gap in the density of states: a so-called hybridization gap. Infrared spectroscopy is ideally suited to probe the electronic processes in heavy fermion systems. All hallmarks of the HF state can be simultaneously probed using this technique. In particular, the Drude-like mode associated with the response of heavy quasiparticles as well as excitations across the hybridization gap have been found and identified as characteristic signatures of the HF state in the IR spectra [107, 143].

The electrodynamic response of heavy fermion metals (HF) has been studied in a large number of systems [107]. Figure 11 displays optical conductivity of UPd_2Al_3 [144, 145]. Above the coherence temperature $T^* = 50 \text{ K}$ ($\chi^2_F(\omega)$) is characterized by a broad Drude-like peak at zero energy. Below $T^* = 50 \text{ K}$, but still above the AFM ordering temperature $T_N = 14 \text{ K}$, two notable features dominate the IR Spectrum of UPd_2Al_3 : a very narrow Drude-like mode and a gap like excitation, with an onset around 50 meV. One also observes a crossing of low- and high- T^* ($\chi^2_F(\omega)$) spectra, with characteristic redistribution of spectral weight. The electronic spectral weight removed from the far-IR part of the spectrum is redistributed both to higher frequencies (above the gap) and to a narrow Drude-like mode at zero frequency. The spectral weight in the Drude mode is smaller but significant since it is ultimately responsible for the metallic behavior of HF at low temperatures. This minuscule spectral weight also indicates that the effective mass of the quasiparticles is enhanced at low temperatures ($m_p^2 \rightarrow 1/m$).

The extended Drude model (Eqs. 4 and 5) has been used frequently for the analysis of correlation effects in HF [146, 147, 148, 149, 107, 143]. The effective mass spectra (Eq. 5) are especially useful in that regard, as the quasiparticle effective mass m^* can be extracted by extrapolating the $m^*(\omega) = m_b$ spectra down to

zero frequency. These so-called optical masses are usually in good agreement with the values obtained using other techniques (specific heat, de Hass–van Alphen, etc.) [147, 107, 143]. In UPd_2Al_3 the effective mass is enhanced by a factor of 35 compared to the band value m_b . Once the system crosses into the AFM ordered state, below $T_N = 14\text{ K}$, a new mode develops around 5 cm^{-1} . This leads to further enhancement of the effective mass to about $50m_b$, in good agreement with specific heat measurements. Similar features were observed in another canonical HF UPt_3 [144, 150], which below 5 K progressively develops into a magnetically ordered state, with extremely small local moments ($0.02\mu_B$) and without long range order.

Hancock *et al.* studied the Kondo systems $\text{YbIn}_{1-x}\text{Ag}_x\text{Cu}_4$ [151], whose properties are believed to be driven by similar physics as in HF metals. In $\text{YbIn}_{1-x}\text{Ag}_x\text{Cu}_4$ silver doping x can be continuously changed over the whole range from 0 to 1. The physical properties of the system also change from a moderately heavy fermion YbAgCu_4 to a mixed-valence YbInCu_4 . For all doping levels the spectra reveal a finite frequency ($2,000\text{ cm}^{-1}$) peak, presumably due to excitations across the hybridization gap. Hancock *et al.* showed that the energy of this mode scales with the square root of the Kondo temperature and concluded that the same underlying physics governs the thermodynamic properties and the formation of this $2,000\text{ cm}^{-1}$ peak. Somewhat different scaling has also been predicted [138] and experimentally observed in non-magnetic HF between the magnitude of hybridization gap and the quasiparticle effective mass $m^* = m_b$ [143]:

$$\frac{m^*}{m_b} = \frac{1}{T}^2; \quad (15)$$

where T is coherence temperature (Fig. 12). This scaling relation reflects the fact that in the low-temperature coherent state of HF the intra-band response (as characterized by $m^* = m_b$) and inter-band response (represented by χ'') are intimately related, at least in the simplest version of the theory. Fig. 12 also includes recently studied d-electron system $\text{Yb}_{14}\text{MnSb}_{11}$, the first case where heavy fermion behavior was discovered by IR spectroscopy [152]. We also note that this scaling between the effective mass and the magnitude of the gap is similar to the scaling in CDW systems Eq. 8, as discussed in Section 5 above. Similar scaling relations are not surprising, knowing that the electrodynamic properties of both systems are described by similar equations [153, 154].

IR spectroscopy has recently been used to study the $f \rightarrow d$ transition in elemental Ce [155]. This rare-earth metal with f-electrons undergoes a phase transition from high temperature to low temperature phase. The nature of this phase transition has been a matter of debate. Reported infrared spectra strongly resemble IR spectra of canonical HF metals. The high- T (β) phase is characterized by a broad and featureless spectrum; in the low- T (α) phase a narrow Drude-like mode and a peak at around 1 eV develop. LDA+DMFT calculations by Haule *et al.* [156] have been able to reproduce both these features. They also revealed that the 1 eV peak is indeed due to excitations across hybridization gap, formed by mixing of f-electrons with conduction electrons.

Holden *et al.* [12] studied the electrodynamic response of a heavy fermion superconductor UBe_{13} , both in the normal and superconducting state. At high temperatures a conventional Drude-like behavior was observed, with essentially frequency independent scattering rate. In the coherent state, but still above $T_c = 0.9\text{ K}$, Holden *et al.* found a development of a very narrow zero-energy mode and a finite frequency peak, presumably due to excitations across a hybridization gap. Finally, in the superconducting state, below T_c , optical spectra revealed marked changes in the low frequency region. In particular, narrowing of the Drude peak and further suppression of optical conductivity χ''_1 (!) compared to normal state values were observed. This behavior is not expected for a dirty limit superconductors and has led Holden *et al.* to suggest that UBe_{13} is a clean limit superconductor.

9 Dimensional crossover in organic and inorganic systems

Many familiar concepts of condensed matter physics are revised in one dimension (1D) [157]. For example, the conventional quasiparticle description breaks down in 1D solids and the spin-charge separation

paradigm needs to be invoked to understand excitations. From a theoretical standpoint, the 1D conductors are interesting in the context of Tomonaga-Luttinger (TL) liquid description predicting unconventional power laws in transport properties and also numerous ground states in systems of coupled 1D chains [158, 159]. An arrangement of coupled 1D conductors is envisioned as a paradigm to explain unconventional properties at higher dimensions specifically in the context to the problem of high- T_c superconductivity [160]. Signatures of 1D transport are being explored in a wide variety of systems including but not limited to carbon nano-tubes, conducting molecules, and semiconducting quantum wires, as well as stripes in high- T_c superconductors and quantum Hall structures. In this section we analyze common characteristics of the electromagnetic response of quasi-1D organic conductors and also of Cu-O chains in high- T_c superconductor of YBCO family.

Infrared conductivity of quasi-1D conductors is highly unconventional [161, 162, 163, 164, 165, 166]. Several groups have investigated the response of linear chains of tetramethyltetrafulvalene (TMTTF)₂X and tetramethyltetraselenafulvalene (TMTSF)₂X, with different interchain counterions X (such as X=AsF₆, PF₆, ClO₄, Br). Charge transfer of one electron from every two (TMTSF)₂X molecules leads to a quarter-filled (or half-filled bands due to dimerization) hole band. In a purely 1D situation this would lead to an insulating (Mott) state. However, Bechgaard salts are better characterized as being only quasi-one-dimensional with finite inter-chain hopping integrals which are distinct in the two transverse directions. Both (TMTTF)₂X and (TMTSF)₂X families of materials as well as other classes of organic quasi-1D conductors typically show high dc conductivity along the direction of the linear chains. One is therefore led to expect a metallic reflectivity in the far infrared. Contrary to this expectation, experiments typically show lower conductivity. The discrepancy between DC and IR results can be resolved assuming the existence of a narrow mode at $\omega = 0$ with the width smaller than the low- ω cut-off of the optical measurements. A direct observation of a mode like this would provide strong argument in favor of collective transport along the conducting chain. Cao *et al.* analyzed the limitations on the spectral weight of this mode and the width of the resonance based on the existing reflectance data [165].

Optical conductivity data are capable of resolving the so-called "dimensionality crossover" in the response of the linear chain compounds [158] as first demonstrated by Vescoli *et al.* [166]. In a purely 1D situation linear chain systems are expected to be in a (Mott) insulating state because of 1/2 or 1/4 filled bands. However this is no longer the case if inter-chain hopping integrals are finite, as is the case in Bechgaard salts. Nevertheless, at high temperatures or frequencies the interchain coupling is diminished thus enabling experimental access to the 1D physics even in a system of weakly coupled chains. The studies of the temperature dependence of the transport properties or of the frequency dependence of the optical conductivity then allow one to explore a crossover from the regimes where 1D physics dominates (high-T, high- ω) to the regime where interchain coupling dominates (low-T, low- ω). The low energy response of (TMTSF)₂X compounds is governed by a correlation gap leading to a sharp increase of the conductivity up to a peak that signifies the magnitude of the gap E_g . This behavior is followed by the power law dependence of the conductivity at higher frequencies predicted theoretically [158, 167]:

$$\sigma(\omega) / \omega^{4n^2 K - 5} \quad (16)$$

where K is the TL-liquid exponent and n is the commensurability. The authors have been able to show that the experimental data indeed follow the power law dependence signaling a crossover to 1D transport in mid-infrared frequencies.

To the best of our knowledge, similar power law scaling is not observed in any inorganic quasi-1D compounds. An interesting exception is the response of the Cu-O chains in PrBa₂Cu₄O₈ discovered by Takenaka *et al.* [168]. In this family of high- T_c cuprates as well as in closely related YBa₂Cu₃O_y compounds CuO₂ bilayers are separated with 1-dimensional Cu-O chains directed along the b-axis. Assuming that the b-axis conductivity can be described as a two-channel process one can isolate the chain response as $\sigma_{ch} = \sigma_b + \sigma_a$ where σ_b and σ_a are the conductivities probed along and across the chain directions respectively. This analysis uncovered the power law behavior of the chain conductivity σ_{ch} consistent with

the response of Bechgaard salts. Lee *et al.* [169] examined scaling dependence of the χ'' spectra for a variety of compounds of $\text{YBa}_2\text{Cu}_3\text{O}_y$ series with $y=6.28-6.75$. Despite the significant doping dependence of the spectra, they all showed a universal behavior when the scaling protocol of Schwartz *et al.* [170] was applied (Fig. 13). The power law reported by Lee *et al.* with $\alpha = 1.5$ in Fig. 14 is distinct from the ω^{-3} response expected for a band insulator [158], but is close to $\alpha = 1.3$ seen in 1D Bechgaard salts [166, 170]. The range of values of the correlation gap E_g in $\text{YBa}_2\text{Cu}_3\text{O}_y$ is comparable to that of the Bechgaard salts as well [166, 170].

Even though the mid-IR response of 1D Cu-O chains in cuprates and that of the organic linear chain compounds uncover common trends the low-frequency behavior of these two classes of 1D conductors is radically different. Specifically, the low-energy collective mode in Bechgaard salt is responsible for less than 1 % of the total spectral weight of the infrared conductivity. In the YBCO system this contribution is as high as 50 %. Lee *et al.* proposed that this discrepancy may originate from strong coupling of the Cu-O chains to the conducting CuO_2 planes [169]. This coupling appears to be enhanced with the increasing doping. The frequency dependence of the collective mode is sensitive to the amount of doping and impurities. At relatively low dopings when chain segments are disordered the collective mode has the form of a finite frequency resonance [169, 171]. Once the chain fragment length exceeds the critical value and the separation between these fragments is reduced, the χ'' (!) spectra reveal the Drude-like metallic behavior which would be impossible in a system of isolated disordered chains. Finally we also note that no scaling has been observed in the in-plane conductivity data of high- T_c cuprates in the stripe ordered state discussed in Section 5. On the other hand, IR measurements of the out-of-plane penetration depth in YBCO have indicated the possibility of a dimensional cross-over from 2D to 3D [172, 173].

10 Summary

Infrared spectroscopy has been instrumental in elucidating a number of interesting effects attributable to strong correlations in solids. In these systems competing interaction often lead to a formation of the energy gap or pseudogap that dominates the electromagnetic response at low energies. Two classes of correlated systems: density wave compounds and heavy fermion conductors reveal correlations between the magnitude of the energy gap and enhancement of quasiparticle effective mass. Despite fundamental differences in the microscopic origins of the gapped state the theoretical description of the electromagnetic response is quite common. One can identify similarities between the spectroscopic fingerprints of pseudogaps in correlated transition metal oxides with the response of the density wave or hybridization gap materials.

Another common attribute of many correlated systems is strong coupling of quasiparticles to collective excitations. Infrared optics uncovered many interesting characteristics of this coupling. An inversion analysis that exemplified here with the high- T_c results is capable of yielding the details of the relevant spectral function. It will be instructive to apply this analysis will be applied to other materials as well. An important virtue of infrared methods in this regard is that this technique is a bulk probe. Other experimental methods capable of investigating strong coupling effects (tunneling, ARPES) are surface sensitive techniques.

Acknowledgements We thank our collaborators T. Timusk, C.C. Homes, J.P. Carbotte, A. Chubukov, L. Degiorgi, W.J. Padilla, K.S. Burch and A. LaForge for useful discussions and critical comments on the manuscript.

References

- [1] P. Drude, *Annalen der Physik* **1**, 566 (1900).
- [2] P. Drude, *Annalen der Physik* **3**, 369 (1900).
- [3] See for example E.J. Singley, K.S. Burch, R. Kawakami, J. Stephens, D.D. Awschalom, D.N. Basov, *Phys. Rev. B* **68**, 165204 (2003).
- [4] G. Kozlov and A. Volov in *Millimeter and Submillimeter Wave Spectroscopy of Solids*, edited by G. Gruner, Springer NY 1998 p.51.
- [5] A. V. Pronin, M. Dressel, A. Pimenov, A. Loidl, I.V. Roshchin and L.H. Greene, *Phys. Rev. B* **57**, 14416 (1998).

- [6] D. Grishkovsky, S. Keiding, M. van Exter, and Ch. Fattinger, *J.Opt.Soc.Am.* **7**, 2006 (1990).
- [7] R.A. Kaindl, M.A. Carnahan, D. Hagele, R. Lovenich, D.S. Chemla, *Nature* **423**, 734 (2003).
- [8] R.D. Averitt and A.J. Taylor, *J.Phys.Cond.Matt.* **14**, 1357 (2002).
- [9] K.S. Burch, J. Stephens, R.K. Kawakami, D.D. Awschalom and D.N. Basov, *Phys.Rev.B* **70** 205208 (2004).
- [10] A.B. Kuzmenko, *Rev.Sci.Instrum.* **76**, 083108 (2005).
- [11] C.C. Homes, M.A. Reedyk, D.A. Crandles and T. Timusk, *Applied Optics* **32**, 2976 (1993).
- [12] A.A.B. Holden, G.M. Wardlaw, M. Reedyk, and J.L. Smith, *Phys.Rev.Lett.* **91**, 136401 (2003).
- [13] D.N. Basov, S.V. Dordevic, E.J. Singley, W.J. Padilla, K.S. Burch, J.E. Elenewski, L.H. Greene, J.Morris and R.Schickling, *Reviews of Scientific Instruments* **74**, 4703 (2003).
- [14] W.J. Padilla, Z.Q.Li, K.S. Burch, Y.S. Lee, K.J. Mikolaitis, and D. N. Basov, *Reviews of Scientific Instruments* **75**, 4710 (2004).
- [15] D.N. Basov and T. Timusk, *Rev.Mod.Phys.* **77**, 721 (2005).
- [16] J.W. Allen and J. C. Mikkelsen, *Phys.Rev.B* **15**, 2952 (1977).
- [17] M. Dressel and G. Gruner, *Electrodynamics of Solids*, (Cambridge University Press, 2001).
- [18] M. Imada, A. Fujimori, and Y. Tokura, *Rev.Mod.Phys.* **70**, 1039 (1998).
- [19] Y. Fujishima, Y. Tokura, T. Arima and S. Uchida, *Phys.Rev.B* **46**, 11167 (1992).
- [20] F. Inaba, T. Arima, T. Ishikawa, T. Katsufuji, and Y. Tokura, *Phys.Rev.B* **52**, 2221 (1995).
- [21] Y. Okimoto, T. Katsufuji, T. Ishikawa, T. Arima, and Y. Tokura, *Phys.Rev.B* **55**, 4206 (1997).
- [22] Y. Tokura, Y. Okimoto, S. Yamaguchi, H. Taniguchi, T. Kimura and H. Takagi, *Phys.Rev.B* **58**, R1699 (1998).
- [23] T. Ido, K. Magoshi, H. Eisaki, and S. Uchida, *Phys.Rev.B* **44**, 12094 (1991).
- [24] S. Uchida, T. Ido and H. Takagi, T. Arima and Y. Tokura S. Tajima, *Phys.Rev.B* **43**, 7942 (1991).
- [25] C.C. Homes, T. Timusk, R. Liang, D.A. Bonn, and W.N. Hardy, *Phys.Rev.Lett.* **71**, 1645 (1993).
- [26] M. J. Rozenberg, G. Kotliar, H. Kajueter, G. A. Thomas, D. H. Rapkine, J. M. Honig, and P. Metcalf, *Phys.Rev.Lett.* **75**, 105 (1995).
- [27] D.N. Basov, H.A. Mook, B. Dabrowski, T. Timusk, *Phys.Rev.B*, **52**, R13141, (1995).
- [28] A. Georges, G. Kotliar, W. Krauth, and M.J. Rozenberg, *Rev.Mod.Phys.* **68**, 13 (1996).
- [29] Y. Tomioka, A. Asamitsu, H. Kuwahara, and Y. Tokura, *Phys.Rev.B*, **53**, R1689 (1996).
- [30] W.F. Brinkman and T.M. Rice, *Phys.Rev.B* **2**, 4302 (1970).
- [31] W. J. Padilla, Y. S. Lee, M. Dumm, G. Blumberg, S. Ono, K. Segawa, S. Komiya, Y. Ando, and D. N. Basov *Phys.Rev.B* **72**, 060511 (2005).
- [32] Y.S. Lee, K. Segawa, Z.Q. Li, W.J. Padilla, M. Dumm, S.V. Dordevic, C.C. Homes, Y. Ando, and D.N. Basov *Phys.Rev.B* **72**, 054529 (2005).
- [33] K. Petukhov and M. Dressel, *Phys.Rev.B* **71**, 073101 (2005).
- [34] G. Gruner, *Density Waves in Solids*, Addison-Wesley, (1994).
- [35] P.A. Lee, T.M. Rice and P.W. Anderson, *Sol.Stat.Comm.* **14**, 703 (1974).
- [36] D. Reagor, S. Sridhar, M. Maki, and G. Gruner *Phys.Rev.B* **32**, 8445 (1985).
- [37] V. Vescoli, L. Degiorgi, H. Berger, and L. Forro, *Phys.Rev.Lett.* **81**, 453 (1998).
- [38] S.V. Dordevic, D.N. Basov, R.C. Dynes and E. Bucher, *Phys.Rev.B* **64**, 161103(R) (2001).
- [39] B. Ruzicka, L. Degiorgi, H. Berger, R. Gaal, and L. Forro, *Phys.Rev.Lett.* **86**, 4136 (2001).
- [40] S.V. Dordevic, D.N. Basov, R.C. Dynes, B. Ruzicka, V. Vescoli, L. Degiorgi, H. Berger, R. Gaal, L. Forro and E. Bucher, *The European Physical Journal B* **33**, 15 (2003).
- [41] D. B. Tanner, K. D. Cummings, and C. S. Jacobsen, *Phys.Rev.Lett.* **47**, 597 (1981).
- [42] G. Travaglini and P. Wachter, *Phys.Rev.B* **30**, 1971 (1984).
- [43] A. W. McConnell, B. P. Clayman, C. C. Homes, M. Inoue, and H. Negishi, *Phys.Rev.B* **58**, 13565 (1998).
- [44] C. C. Homes and J. E. Eldridge, *Phys.Rev.B* **42**, 9522 (1990).
- [45] G. Minton and J. W. Brill, *Phys.Rev.B* **36**, 4254 (1987).
- [46] C. S. Jacobsen, D. B. Tanner, and K. Bechgaard, *Phys.Rev.B* **28**, 7019 (1983).
- [47] C. C. Homes, J. L. Musfeldt, and D. B. Tanner, *Phys.Rev.B* **48**, 16799 (1993).
- [48] W. N. Creager, P. L. Richards, and A. Zettl, *Phys.Rev.B* **44**, 3505 (1991).
- [49] P. Calvani, G. De Marzi, P. Dore, S. Lupi, P. Maselli, F. D'Amore, S. Gagliardi, and S-W. Cheong, *Phys.Rev.Lett.* **81**, 4504 (1998).
- [50] Z.-T. Zhu, J. L. Musfeldt, Z. S. Teweldemedhin, and M. Greenblatt, *Phys.Rev.B* **65**, 214519 (2002).
- [51] M. Rice, *Phys.Rev.Lett.* **37**, 36 (1976).
- [52] H. Fehske, M. Kinatder, G. Wellein, and A. R. Bishop, *Phys.Rev.B* **63**, 245121 (2001).
- [53] B. R. Jones, A. B. Sushkov, J. L. Musfeldt, Y. J. Wang, A. Revcolevschi, and G. Dhalenne, *Phys.Rev.B* **63**, 134414 (2001).
- [54] A. B. Sushkov, O. Tchernyshyov, W. R. II, S. W. Cheong, and H. D. Drew, *Phys.Rev.Lett.* **94**, 137202 (2005).
- [55] A.S. Barker, Jr., B.I. Halperin, and T.M. Rice, *Phys.Rev.Lett.* **20**, 384 (1968).
- [56] D.N. Basov, E.J. Singley, S.V. Dordevic, *Phys.Rev.B* **65**, 054516 (2002).

- [57] Ar. Abanov and A. V. Chubukov, Phys.Rev.Lett. **88**, 217001 (2002).
- [58] A. V. Chubukov, Ar. Abanov, and D. N. Basov, Phys.Rev.B **68**, 024504 (2003).
- [59] E. W. Carlson, V. J. Emery, S. A. Kivelson, and D. Orgad, in *The Physics of Conventional and Unconventional Superconductors*, ed. by K. H. Bennemann and J. B. Ketterson (Springer-Verlag); S.A. Kivelson, I.P. Bindloss, E. Fradkin, V. Oganessian, J.M. Tranquada, A. Kapitulnik, and C. Howald, Rev.Mod.Phys. **75**, 1201 (2003).
- [60] S. Tajima N.L. Wang, N. Ichikawa, H. Eisaki, S. Uchida, H. Kitano T. Hanaguri and A. Maeda, Europhys.Lett. **47**, 715 (1999).
- [61] M. Dumm, D. N. Basov, S. Komiya, Y. Abe, and Y. Ando, Phys.Rev.Lett. **88**, 147003 (2002).
- [62] M. Matsuda, M. Fujita, K. Yamada, R. J. Birgeneau, M. A. Kastner, H. Hiraka, Y. Endoh, S. Wakimoto and G. Shirane, Phys.Rev.B **62**, 9148 (2000).
- [63] M. Dumm, Seiki Komiya, Yoichi Ando, D.N. Basov, Phys.Rev.Lett. **91**, 077004 (2003).
- [64] A. Zimmers, J.M. Tomczak, R.P.S.M. Lobo, N. Bontemps, C.P. Hill, M.C. Barr, Y. Dagan, R. L. Greene, A.J. Millis and C.C. Homes, Europhys.Lett. **70**, 225 (2005).
- [65] Y. Onose, Y. Taguchi, K. Ishizaka and Y. Tokura, Phys.Rev.B **69** 024504 (2004).
- [66] N. L. Wang, G. Li, Dong Wu, X. H. Chen, C. H. Wang, H. Ding, cond-mat/0410242.
- [67] S. Chakravarty, R. B. Laughlin, D. K. Morr, and C. Nayak, Phys.Rev.B **63**, 094503 (2001).
- [68] B. Valenzuela, E.J. Nicol, and J.P. Carbotte, Phys.Rev.B **71**, 134503 (2005).
- [69] R. Gerami and Ch. Nayak, cond-mat/0506237.
- [70] T. Osafune, N. Motoyama, H. Eisaki, S. Uchida and S. Tajima, Phys.Rev.Lett. **82**, 1313 (1999).
- [71] D.N. Basov, B. Dabrowski and T. Timusk, Phys.Rev.Lett. **81**, 2132 (1998).
- [72] T. Vuletic, B. Korin-Hamzic, S. Tomic, B. Gorshunov, P. Haas, T. Room, M. Dressel, J. Akimitsu, T. Sasaki, and T. Nagata, Phys.Rev.Lett. **90** 257002, (2003).
- [73] Y.S. Lee, J.S. Lee, K.W. Kim, T.W. Noh, Jaejun Yu, E.J. Choi, G. Cao and J.E. Crow, Europhys.Lett. **55** 280 (2001).
- [74] G. Cao, J.E. Crow, R.P. Guertin, P.F. Henning, C.C. Homes, M. Strongin, D.N. Basov, E. Lochner, Sol.Stat.Comm. **113**, 657 (2000).
- [75] K. Takada, H. Sakurai, E. Takayama-Muromachi, F. Izumi, R. A. Dilanian, and T. Sasaki, Nature **422**, 53 (2003).
- [76] S. Lupi, M. Ortolani, and P. Calvani, Phys.Rev.B **69**, 180506(R) (2004).
- [77] J. Hwang, J. Yang, T. Timusk and F.C. Chou, cond-mat/0405200.
- [78] G. Caimi, L. Degiorgi, H. Berger, N. Barisic, L. Forro, and F. Bussy, Eur.Phys.J. B **40**, 231 (2004).
- [79] N.L.Wang, Dong Wu, G. Li, X.H. Chen, C.H. Wang, and X.G. Luo, Phys.Rev.Lett. **93**, 147403 (2004).
- [80] C. Bernhard, A.V. Boris, N. N. Kovaleva, G. Khaliullin, A.V. Pimenov, Li Yu, D. P. Chen, C.T. Lin, and B. Keimer, Phys.Rev.Lett. **93**, 167003 (2004).
- [81] Z. Schlesinger, R. T. Collins, F. Holtzberg, C. Feild, S. H. Blanton, U. Welp, G. W. Crabtree, Y. Fang and J. Z. Liu, Phys.Rev.Lett. **65**, 801 (1990).
- [82] A. El Azrak, R. Nahoum, N. Bontemps M. Guilloux-Viry, C. Thivet, A. Perrin, S. Labdi, Z. Z. Li, and H. Raffy Phys.Rev.B **49**, 9846 (1994).
- [83] D. van der Marel, H.J.A. Molegraaf, J. Zaanen, Z. Nussinov, F. Carbone, A. Damascelli, H. Eisaki, M. Greven, P.H. Kes, M. Li, Nature **425**, 271 (2003).
- [84] P. Kostic, Y. Okada, N. C. Collins, and Z. Schlesinger, J. W. Reiner, L. Klein, A. Kapitulnik, T. H. Geballe, and M. R. Beasley, Phys.Rev.Lett. **81**, 2498 (1998).
- [85] J. S. Dodge, C. P. Weber, J. Corson, J. Orenstein, Z. Schlesinger, J. W. Reiner, and M. R. Beasley, Phys.Rev.Lett. **85**, 4932 (2000).
- [86] Y. S. Lee, Jaejun Yu, J. S. Lee, T. W. Noh, T.-H. Gimm, Han-Yong Choi and C. B. Eom, Phys.Rev.B **66**, 041104 (2002).
- [87] F.P. Mena, D. van der Marel, A. Damascelli, M. Fath, A.A. Menovsky, and J.A. Mydosh, Phys.Rev.B **67**, 241101 (2003).
- [88] L.B. Ioffe and A.J. Millis, Phys.Rev.B **58**, 11631 (1998).
- [89] P.B. Littlewood and C.M. Varma, J.Appl.Phys. **69**, 4979 (1991).
- [90] J. Hwang, T. Timusk, A. V. Puchkov, N. L. Wang, G. D. Gu, C. C. Homes, J. J. Tu and H. Eisaki, Phys.Rev.B **69**, 94520 (2004).
- [91] A. Carrington, A.P. Mackenzie, C.T. Lin, and J.R. Cooper, Phys.Rev.Lett. **69**, 2855 (1992).
- [92] B.P. Stojkovic and D. Pines, Phys.Rev.Lett. **76**, 811 (1996).
- [93] R. Hlubina and T.M. Rice, Phys.Rev.B **51**, 9253 (1995).
- [94] A. Damascelli, Z. Hussain, and Z.-X. Shen, Rev.Mod.Phys. **75**, 473 (2003).
- [95] L.B. Ioffe, and A.J. Millis, Science **285**, 1241 (1999).
- [96] A.V. Chubukov, D. Pines and J. Schmalian, in *The Physics of Superconductors*, edited by K.H. Bennemann and J.B.Ketterson (Springer Berlin) v.1, p.495.

- [97] Ar. Abanov, A.V. Chubukov and J. Schmalian, *Advances in Physics* **52**, 119 (2003).
- [98] M.M. Zemljic and P. Prelovsek, *cond-mat/0504640*.
- [99] G. Baskaran, Z. Zou, and P. W. Anderson, *Solid State Commun.* **63**, 973 (1987).
- [100] V. Emery and S. Kivelson, *Nature (London)* **374**, 434 (1995).
- [101] L. B. Ioffe and G. Kotliar, *Phys. Rev. B* **42**, 10348 (1990).
- [102] P.W. Anderson, *Phys. Rev. B.* **55**, 11785 (1997).
- [103] S. L. Sondhi, S. M. Girvin, J. P. Carini, and D. Shahar, *Rev.Mod.Phys.* **69**, 315 (1997).
- [104] S. Sachdev, *Quantum Phase Transitions*, Cambridge University Press (1999).
- [105] P. Coleman and A. Schofield, *Nature* **433**, 226 (2005).
- [106] Degiorgi, L., St. Thieme, H. R. Ott, M. Dressel, G. Gruner, Y.Dalichaouch, M. B. Maple, Z. Fisk, C. Geibel, and F. Steglich, *Z.Phys.B* **102**, 367 (1997).
- [107] L. Degiorgi, *Rev.Mod.Phys.* **71**, 687 (1999).
- [108] G.R. Stewart, *Rev.Mod.Phys.* **71** 797 (2001).
- [109] P.V. Bogdanov, A. Lanzara, S.A. Kellar, X.J. Zhou, E.D. Lu, W.J. Zheng, G. Gu, J.-I. Shimoyama, K. Kishio, H. Ikeda, R. Yoshizaki, Z. Hussain and Z.X. Shen, *Phys.Rev.Lett.* **85**, 2581 (2000).
- [110] A. Lanzara, P.V. Bogdanov, X.J. Zhou, S.A. Kellar, D.L. Feng, E.D. Lu, T. Yoshida, H. Eisaki, A. Fujimori, K. Kishio, J.-I. Shimoyama, T. Noda, S. Uchida, Z. Hussain, Z.-X. Shen, *Nature* **412**, 510 (2001).
- [111] Z.-X. Shen, *cond-mat/0305576*.
- [112] X.J. Zhou, T. Yoshida, A. Lanzara, P.V. Bogdanov, S.A. Kellar, K.M. Shen, W.L. Yang, F. Ronning, T. Sasagawa, T. Kakeshita, T. Noda, H. Eisaki, S. Uchida, C.T. Lin, F. Zhou, J.W. Xiong, W.X. Ti, Z.X. Zhao, A. Fujimori, Z. Hussain, and Z.-X. Shen, *Nature* **423**, 398 (2003).
- [113] D. Pines, *Physica B* **163**, 78 (1990).
- [114] J.P. Carbotte, E. Schachinger and D.N. Basov, *Nature* **401**, 354 (1999).
- [115] D. Munzar, C. Bernhard and M. Cardona, *Physica C* **312**, 121 (1999).
- [116] Ar. Abanov, A.V. Chubukov, M. Eschrig, M.R. Norman, and J. Schmalian, *Phys.Rev.Lett.* **89**, 177002 (2002).
- [117] Hae-Young Kee, S.A. Kivelson, and G. Aeppli, *Phys.Rev.Lett.* **88**, 257002 (2002).
- [118] A.V. Chubukov and M.R. Norman, *cond-mat/0402304*.
- [119] D.N. Basov, R. Liang, B. Dabrowski, D.A. Bonn, W.N. Hardy, T. Timusk, *Phys.Rev.Lett.* **77**, 4090 (1996).
- [120] A.V. Puchkov, D.N. Basov and T. Timusk, *J.Phys.C* **8**, 10049 (1996).
- [121] A. V. Puchkov, P. Fournier, D. N. Basov, T. Timusk, A. Kapitulnik, and N. N. Kolesnikov, *Phys.Rev.Lett.* **77**, 3212 (1996).
- [122] S.V. Dordevic, C.C. Homes, J.J. Tu, T. Valla, M. Strongin, P.D. Johnson, G.D. Gu and D.N. Basov, *Phys.Rev.B* **71**, 104529 (2005).
- [123] P.B. Allen, *Phys.Rev.B* **3**, 305 (1971).
- [124] A. J. Millis, S. Sachdev, and C. M. Varma, *Phys.Rev.B* **37**, 4975 (1988).
- [125] S.V. Shulga, O.V. Dolgov and E.G. Maksimov, *Physica C* **178**, 266 (1991).
- [126] F. Marsiglio, T. Startseva and J.P. Carbotte, *Physics Letters A* **245**, 172 (1998).
- [127] J.J. Tu, C.C. Homes, G.D. Gu, D.N. Basov and M. Strongin, *Phys.Rev.B* **66**, 144514 (2002).
- [128] N.L. Wang, P. Zheng, J.L. Luo, Z.J. Chen, S.L. Yan, L. Fang, Y.C. Ma, *Phys.Rev.B* **68**, 054516 (2003).
- [129] P. Casek, Ch. Bernhard, J. Humlicek and D. Munzar, *cond-mat/0503666*.
- [130] S.G. Sharapov, J.P. Carbotte, *cond-mat/0505304*.
- [131] J. Hwang, J. Yang, T. Timusk, S.G. Sharapov, J.P. Carbotte, D.A. Bonn, Ruixing Liang and W.N. Hardy, *cond-mat/0505302*.
- [132] M.R. Norman and H. Ding, *Phys.Rev.B* **57** R11089 (1998).
- [133] Ar. Abanov, A.V. Chubukov, and J. Schmalian, *Phys.Rev.B* **63**, 180510 (2001).
- [134] J.P. Carbotte and E. Schachinger, this volume.
- [135] A.V. Chubukov, private communication.
- [136] J. Hwang, T. Timusk, G.D. Gu, *Nature* **427**, 714 (2004).
- [137] N.P. Armitage, D.H. Lu, C. Kim, A. Damascelli, K.M. Shen, F. Ronning, D.L. Feng, P. Bogdanov, X.J. Zhou, W.L. Yang, Z. Hussain, P.K. Mang, N. Kaneko, M. Greven, Y. Onose, Y. Taguchi, Y. Tokura, and Z.-X. Shen, *Phys.Rev.Lett.* **68** 064517 (2003).
- [138] A.J. Millis and P.A. Lee, *Phys.Rev.B* **35**, 3394 (1987).
- [139] A.J. Millis, M. Lavagna and P.A. Lee, *Phys.Rev.B* **36**, 864 (1987).
- [140] P. Coleman, *Phys.Rev.Lett.* **59**, 1026 (1987).
- [141] P. Fulde, *Electron Correlations in Molecules and Solids* Second Edition, (Springer-Verlag, Berlin, 1993).
- [142] A.C. Hewson, *The Kondo Problem to Heavy Fermions*, (Cambridge University Press, Cambridge, 1997).
- [143] S.V. Dordevic, D.N. Basov, N.R. Dilley, E.D. Bauer and M.B. Maple, *Phys.Rev.Lett.* **86**, 684 (2001).
- [144] M. Dressel, N. Kasper, K. Petukhov, B. Gorshunov, G. Gruner, M. Huth, and H. Adrian, *Phys.Rev.Lett.* **88**, 186404 (2002).

- [145] M. Dressel, N. Kasper, K. Petukhov, D.N. Peligrad, B. Gorshunov, M. Jourdan, M. Huth, and H. Adrian, Phys.Rev.B **66**, 035110 (2002).
- [146] B.C. Webb, A.J. Sievers and T. Mihalisin, Phys.Rev.Lett. **57**, 1951 (1986).
- [147] D.A. Bonn, J.D. Garrett, and T. Timusk, Phys.Rev.Lett. **61**, 1305 (1988).
- [148] P. Wachter, in *Handbook on the Physics and Chemistry of Rare Earths*, Vol. **19**, edited by K.A.Gschneidner and LeRoy Eyring, (Elsevier Science, Amsterdam, New York, 1994).
- [149] S. Donovan, A. Schwartz, and G. Gruner, Phys.Rev.Lett. **79**, 1401 (1997).
- [150] P. Tran, S. Donovan, and G. Gruner, Phys.Rev.B **65**, 205102 (2002).
- [151] J.N. Hancock, T. McKnew, Z. Schlesinger, J.L. Sarrao and Z. Fisk, Phys.Rev.Lett. **92**, 186405 (2004).
- [152] K.S. Burch, A. Schafgans, N.P. Butch, T.A. Sayles, M.B. Maple, B.C. Sales, D. Mandrus and D.N. Basov, Phys.Rev.Lett. **94**, 046401 (2005).
- [153] T. Portengen, Th. Ostreich, and L. J. Sham, Phys.Rev.Lett. **76**, 3384 (1996).
- [154] T. Portengen, Ph.D. thesis, University of California, San Diego.
- [155] J.W. van der Eb, A.B. Kuz'menko, and D. van der Marel, Phys.Rev.Lett. **86**, 3407 (2001).
- [156] K. Haule, V. Oudovenko, S.Y. Savrasov, and G. Kotliar Phys.Rev.Lett. **94**, 036401 (2005).
- [157] M. Dressel, Naturwissenschaften **90**, 337(2003).
- [158] T. Giamarchi, Physica B **230-232**, 975 (1997), and references therein.
- [159] D. Controzzi, F.H.L. Essler, and A.M. Tsvelik, Phys.Rev.Lett. **86**, 680 (2001).
- [160] David G. Clarke, S.P. Strong, and P.W. Anderson, Phys.Rev.Lett. **72**, 3218 (1994).
- [161] D.B. Tanner, C.S. Jacobsen, A.F. Garito and A.J. Heeger, **13**, 3381 (1976).
- [162] C.S. Jacobsen, D.B. Tanner, and K. Bechgaard, Phys.Rev.B **28**, 7019 (1983).
- [163] H.K. Ng, T. Timusk, and K. Bechgaard, Phys.Rev.B **30**, 5842 (1984).
- [164] H.K. Ng, T. Timusk, D. Jerome, and K. Bechgaard, Phys.Rev.B **32**, 8041 (1985).
- [165] N. Cao, T. Timusk and K. Bechgaard, J.Phys.I France **6**, 1719 (1996).
- [166] V. Vescoli, L. Degiorgi, W. Henderson, G. Gruner, K.P. Starkey and L.K. Montgomery, Science **281**, 1181 (1998).
- [167] T. Giamarchi, Chemical Rev. **104**, 5037 (2004).
- [168] K. Takenaka, K. Nakada, A. Osuka, S. Horii, H. Ikuta, I. Hirabayashi, S. Sugai, and U. Mizutani, Phys.Rev.Lett. **85**, 5428 (2000).
- [169] Y.-S Lee, Kouji Segawa, Yoichi Ando, and D.N. Basov, Phys.Rev.Lett. **94**, 137004 (2005).
- [170] A. Schwartz, M. Dressel, G. Gruner V. Vescoli, L. Degiorgi and T. Giamarchi, Phys.Rev.B **58**, 1261 (1998).
- [171] C.C. Homes, D.A. Bonn, Ruixing Liang, W.N. Hardy, D.N. Basov, T. Timusk and B.P. Clayman, Phys.Rev.B **60**, 9782 (1999).
- [172] C. C. Homes, S. V. Dordevic, M. Strongin, D. A. Bonn, Ruixing Liang, W. N. Hardy, Seiki Komiya, Yoichi Ando, G. Yu, N. Kaneko, X. Zhao, M. Greven, D. N. Basov and T. Timusk, Nature **430**, 539 (2004).
- [173] C.C. Homes, S.V. Dordevic, D.A. Bonn, Ruixing Liang, W.N. Hardy and T. Timusk, Phys.Rev.B **71**, 184515 (2005).

Fig. 1 The energy scales of certain phenomena in condensed matter systems with strongly correlated electrons. Most of these energies are in the microwave, infrared, visible and ultraviolet parts of the spectrum. Infrared spectroscopy, combined with microwave and optical spectrometry can be used to probe all these phenomena simultaneously.

Fig. 2 The optical conductivity of several doped transition metal insulators: $\text{La}_{1-x}\text{Sr}_x\text{TiO}_3$ [19], $\text{La}_{1-x}\text{Sr}_x\text{VO}_3$ [20], $\text{La}_{1-x}\text{Sr}_x\text{MnO}_3$ [21], $\text{La}_{1-x}\text{Sr}_x\text{CoO}_3$ [22], $\text{La}_{2-x}\text{Sr}_x\text{NiO}_4$ [23], and $\text{La}_{2-x}\text{Sr}_x\text{CuO}_4$ [24]. The panels are arranged according to the number of d electrons of transition metals, starting with Ti with electron configuration $[\text{Ar}]3d^24s^2$, until Cu with configuration $[\text{Ar}]3d^{10}4s$. In all systems as doping x increases the gap is filled, as the spectral weight from the region above the gap is transferred below the gap and into the Drude-like mode.

Fig. 3 Energy dependence of the carrier effective mass m^* in $\text{Sr}_{1-x}\text{La}_x\text{TiO}_3$ (left panel) [19], $\text{La}_{2-x}\text{Sr}_x\text{CuO}_4$ [31] and $\text{YBa}_2\text{Cu}_3\text{O}_y$ [32] obtained from the extended Drude model. The diagram shows a strong enhancement of m^* values in the titanate, but not in cuprates. The upper panels show the doping dependence of the optical effective mass $m^* = m^*(\omega \rightarrow 0)$. The top middle and right panles also display the optical mass values extracted from a combination of the optical and Hall data as detailed in [31]. All data is taken at room temperature.

Fig. 4 The scattering rate $1/\tau(\omega)$ and optical conductivity $\sigma_1(\omega)$ (inset) of metallic chromium [56] at 10 and 312 K. Chromium is a canonical example of a 3D SDW system with $T_{SDW} = 312$ K. Above the transition the optical constants display typical metallic behavior, with a Drude-like mode in $\sigma_1(\omega)$ and ω^{-2} dependence of $1/\tau(\omega)$ expected within Landau Fermi liquid theory. At 10 K the spectra show deviations from this canonical behavior: the conductivity reveals gap-like suppression between 200–700 cm^{-1} and narrowing of the zero-energy mode. This results in suppression of scattering rate at low frequencies and characteristic overshoot around 900 cm^{-1} .

Fig. 5 Scaling between the optical gap and the effective mass m^* in various CDW and SDW systems [34, 35, 36, 17]. The scaling defined by Eq. 8 was proposed by Lee, Rice and Anderson [35]. The scaling is followed by a number of "conventional" CDW and SDW materials, but also by some transition metal oxides with charge and/or spin ordered states.

Fig. 6 Universal power laws of the optical conductivity spectra of a nearly optimally doped high- T_c superconductor $\text{Bi}_2\text{Sr}_2\text{Ca}_{0.92}\text{Y}_{0.08}\text{Cu}_2\text{O}_8$ with $T_c = 88$ K. In (a) the absolute values of the optical conductivity $\sigma_1(\omega)$ are plotted on a double logarithmic scale. The open symbols correspond to the power law $\sigma_1(\omega) \propto \omega^{-0.65}$. In (b) the phase angle function of the optical conductivity $\arctan(\sigma_2/\sigma_1)$ described in the text is presented. From van der Marel *et al.* [83].

Fig. 7 Logarithmic plot of the optical conductivity of SrRuO_3 obtained by three methods, over three decades ranges of frequency. The conductivity obtained from the infrared reflectivity at 40 K is indicated by the long dashed line. Results from the far-infrared transmission measurements, as described in the text, are indicated by solid lines, and THz measurements by short dashed lines, with both sets ordered in temperature from top to bottom with $T = 8, 40, 60$, and 80 K. Least-squared fits to $\sigma_1(\omega) = A/(1 + i\omega/\omega_c)$ using only THz data are shown by dotted lines. Inset: temperature dependence of ω_c obtained for $\omega_c = 0.4$ (closed circles), compared to quadratic temperature dependence of the relaxation rate. From Dodge *et al.* [85].

Fig. 8 The electron-boson spectral function $\omega^2 F(\omega)$ for optimally doped cuprate $\text{YBa}_2\text{Cu}_3\text{O}_{6.95}$ (full line) and the spin excitation spectrum $\chi''(\omega)$ (full symbols) [114]. The $\omega^2 F(\omega)$ spectrum was obtained using Eq. 12 and $\chi''(\omega)$ is from neutron scattering experiments. Eq. 12 does not take into account a gap in the density of states, which results in unphysical negative values in the spectral function. From Carbotte *et al.* [114].

Fig. 9 The inversion calculations of the electron-boson spectral function $\omega^2 F(\omega)$ with the formula with the gap Eq. 13 for optimally doped $\text{YBa}_2\text{Cu}_3\text{O}_{6.95}$ (the same as in Fig. 8) [122]. The left panels display $\omega^2 F(\omega)$ and the right panels scattering rate data $1/\tau(\omega)$ and $1/\tau_{ca1}(\omega)$ calculated from the spectral function on the left. For $\Delta = 0$ the result displays strong negative deep, but as Δ increases, the deep is progressively suppressed. These calculations illustrate that the origin of the negative value in the spectral function is directly related to the gap in the DOS. Negative values can be eliminated when the appropriate energy gap is used.

Fig. 10 The electron-boson spectral function $\omega^2 F(\omega)$ for underdoped high- T_c superconductor $\text{YBa}_2\text{Cu}_3\text{O}_{6.65}$ with $T_c \approx 60$ K. The top panel display $\omega^2 F(\omega)$ calculated from the scattering rate $1/\tau(\omega)$ using Eqs. 10 or 11 [122]. The bottom panel shows $\omega^2 F(\omega)$ calculated from the corresponding effective mass $m^*(\omega) = m_b$ spectra using Eq. 14. In each panel, different curves represent calculations with different number of singular values, as explained in [122]. Eqs. 10, 11 and 14 do not take into account a gap in the density of states, which results in unphysical negative values.

Fig. 11 The optical conductivity of a heavy fermion system UPd_2Al_3 [144, 145]. Above coherence temperature $T_c \approx 50$ K, the spectrum displays conventional behaviour in the form of a broad Drude mode. Below $T_c \approx 50$ K two distinctive feature develop in the spectra: Drude-like mode at zero frequency and gap-like excitations with an onset at around 50 meV. In addition, below AFM ordering temperature $T_N = 14$ K a new finite frequency mode develops at around 5 cm^{-1} , which causes further enhancement of the effective mass.

Fig. 12 Scaling between the quasiparticle effective mass $m^* = m_b$ and the magnitude of hybridization gap Δ in a number of heavy fermion systems [143]. The line represents $m^* = m_b = (\Delta/T_c)^2$ relation, where T_c is the coherence temperature. Notably, heavy fermion systems with magnetic order do not fall on the scaling line. Similar scaling between the optical gap and the effective mass has also been discussed for CDW systems (Fig. 5).

Fig. 13 The frequency-dependent conductivities of $(\text{TMTSF})_2\text{X}$ ($\text{X}=\text{PF}_6$, AsF_6 , and ClO_4) obtained in the polarization along the conducting linear chains. Both axes have been normalized to the peak of the finite energy mode near 200 cm^{-1} . The universal behavior of the real part of the conductivity $\sigma_1(\omega)$. From Schwartz *et al.* [170].

Fig. 14 Spectra of $\chi''(\omega) = \chi''_{pb}(\omega) - \chi''_{pa}(\omega)$ at lowest temperatures for a series of YBCO crystals. For $y = 6.75$, the coherent mode is not visible because its weight is transferred to superconducting δ -peak at $\omega = 0$. (b) $\chi''(\omega) = \chi''_{peak}$ with $\omega = \omega_{peak}$ as the abscissa. For clarity, the sharp phonon structures are removed from the data in the bottom panel. The solid line represents ω -dependence with $\gamma = 1.6$.

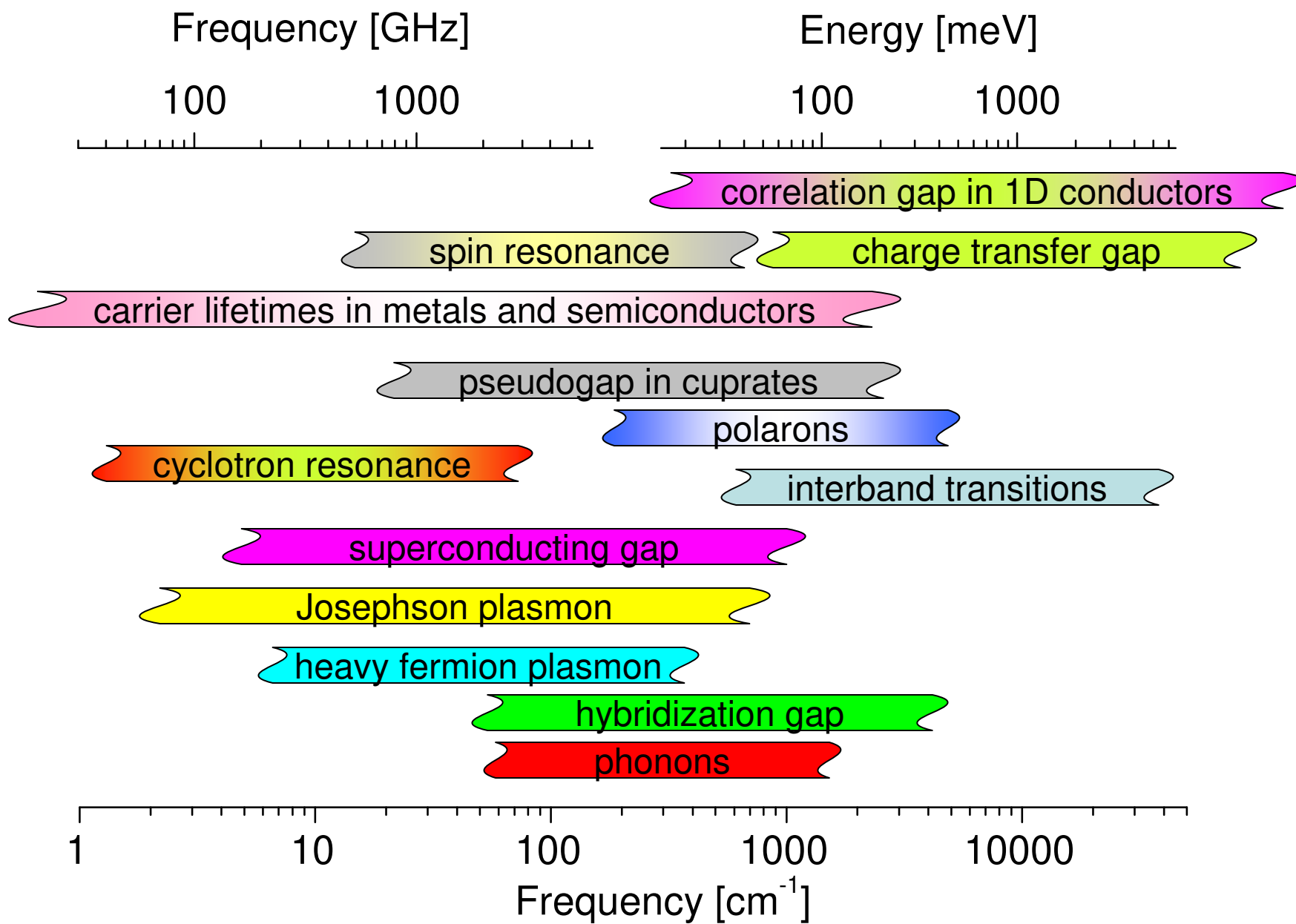
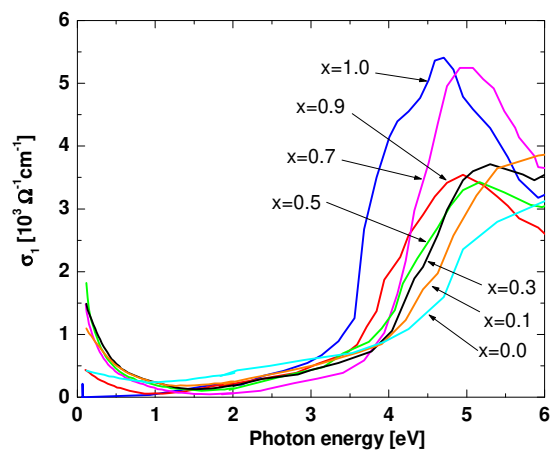
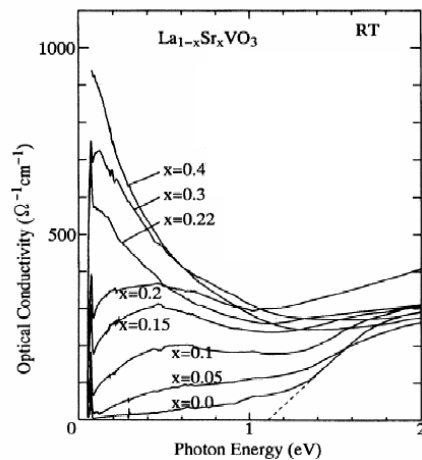


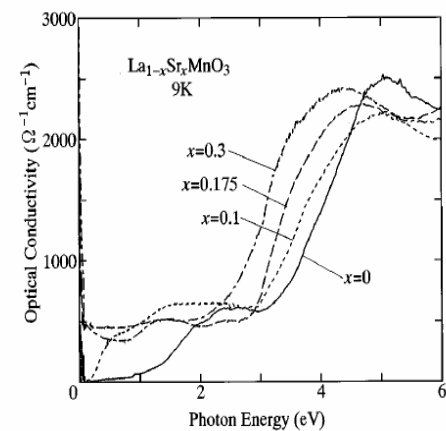
Figure 1



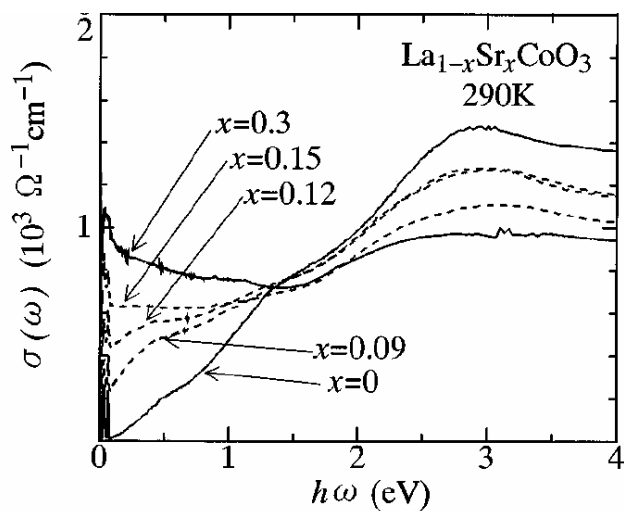
$\text{La}_{1-x}\text{Sr}_x\text{TiO}_3$



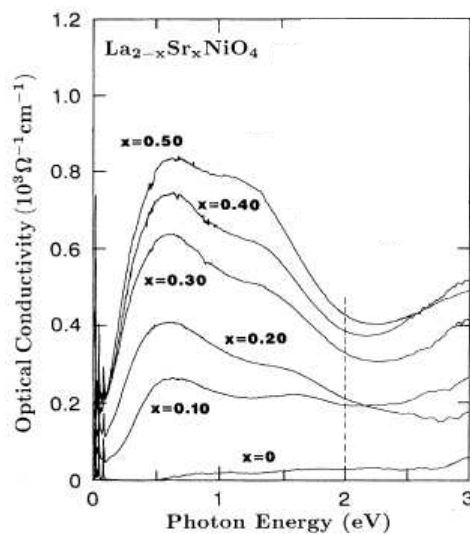
$\text{La}_{1-x}\text{Sr}_x\text{VO}_3$



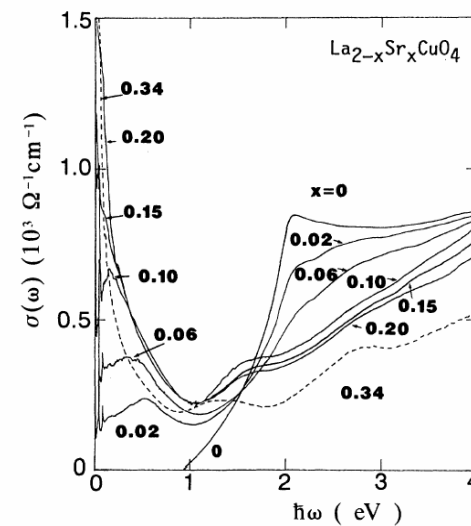
$\text{La}_{1-x}\text{Sr}_x\text{MnO}_3$



$\text{La}_{1-x}\text{Sr}_x\text{CoO}_3$



$\text{La}_{2-x}\text{Sr}_x\text{NiO}_4$



$\text{La}_{2-x}\text{Sr}_x\text{CuO}_4$

Figure 2

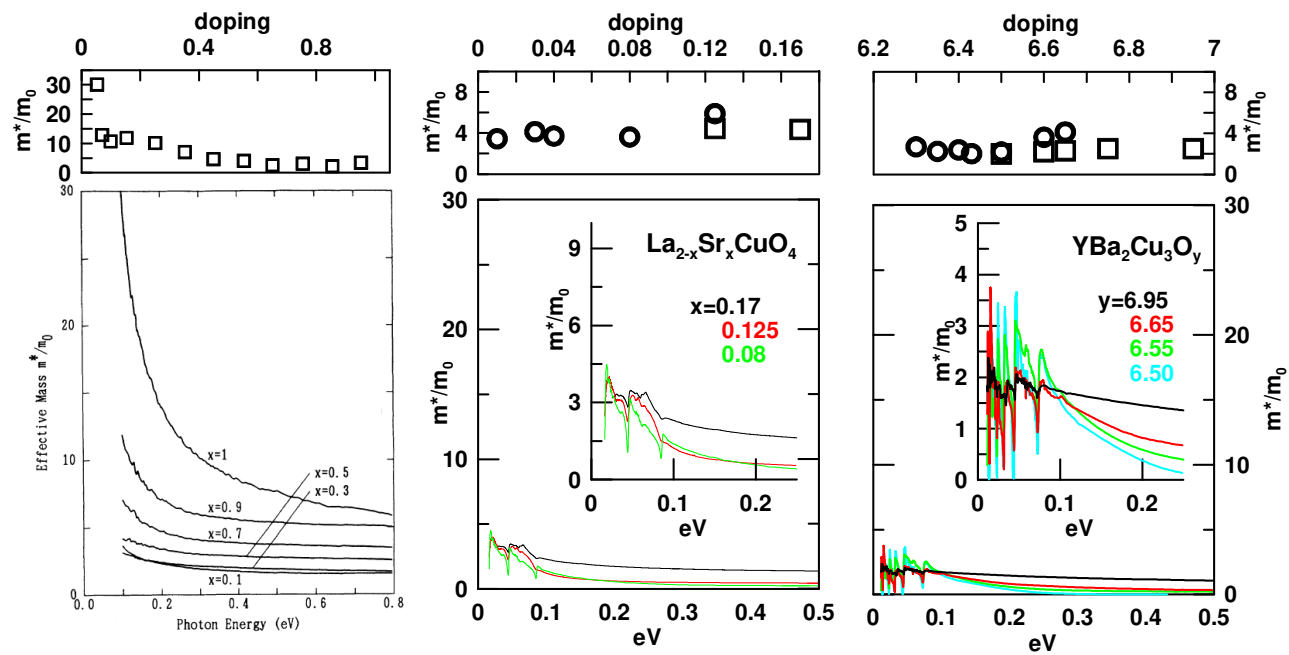


Figure 3

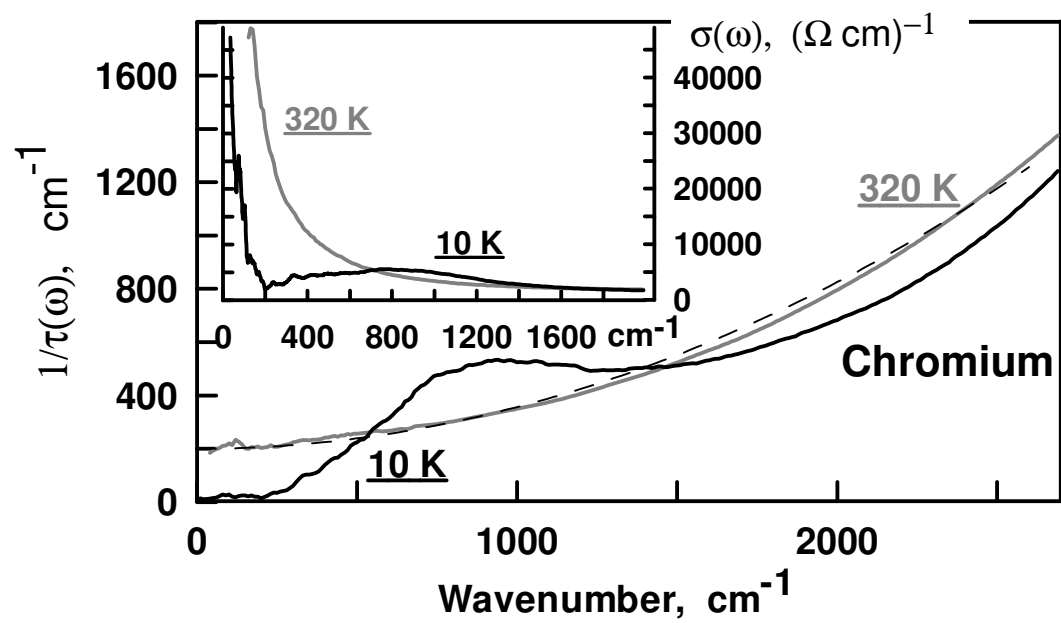


Figure 4



Figure 5

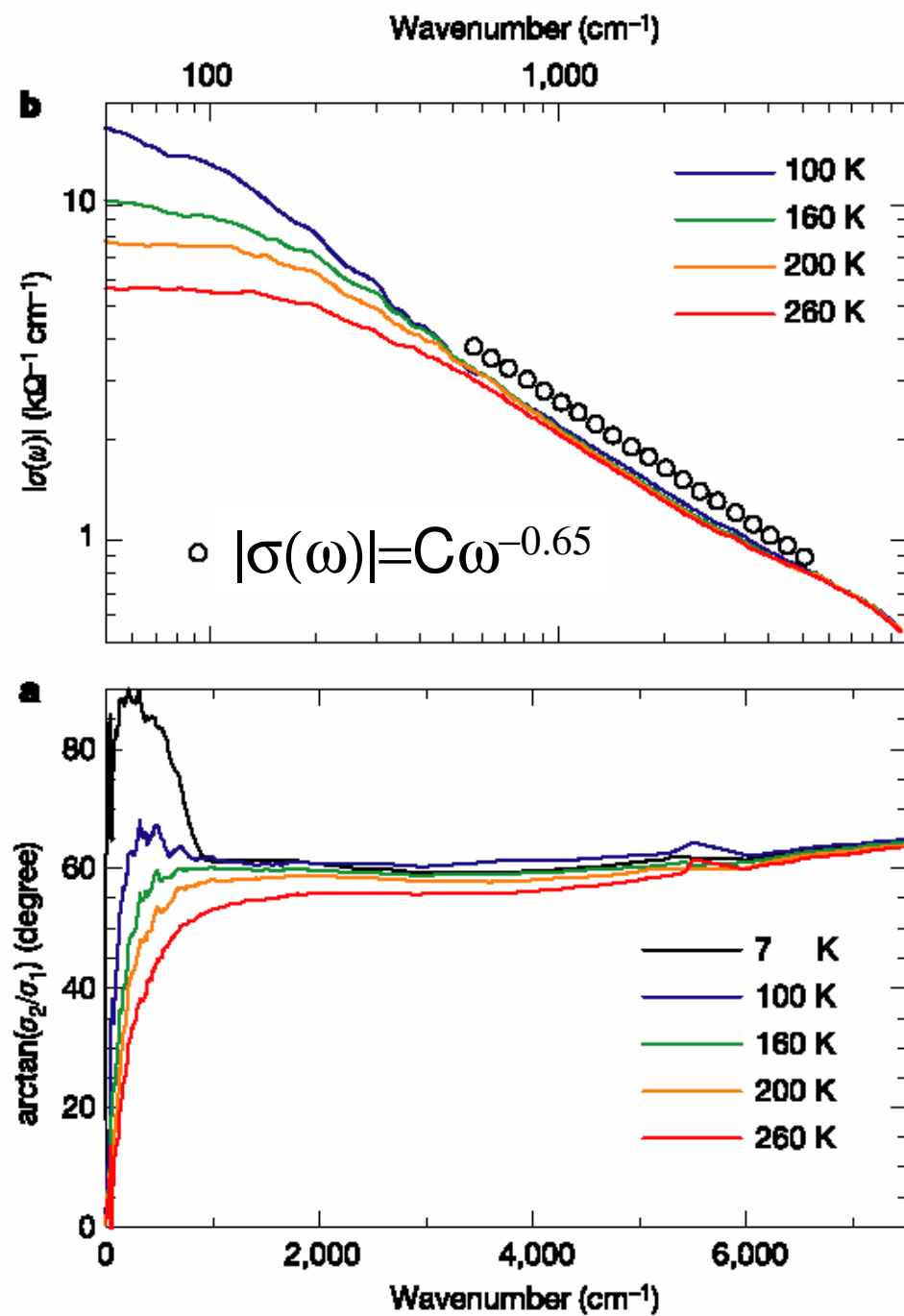


Figure 6

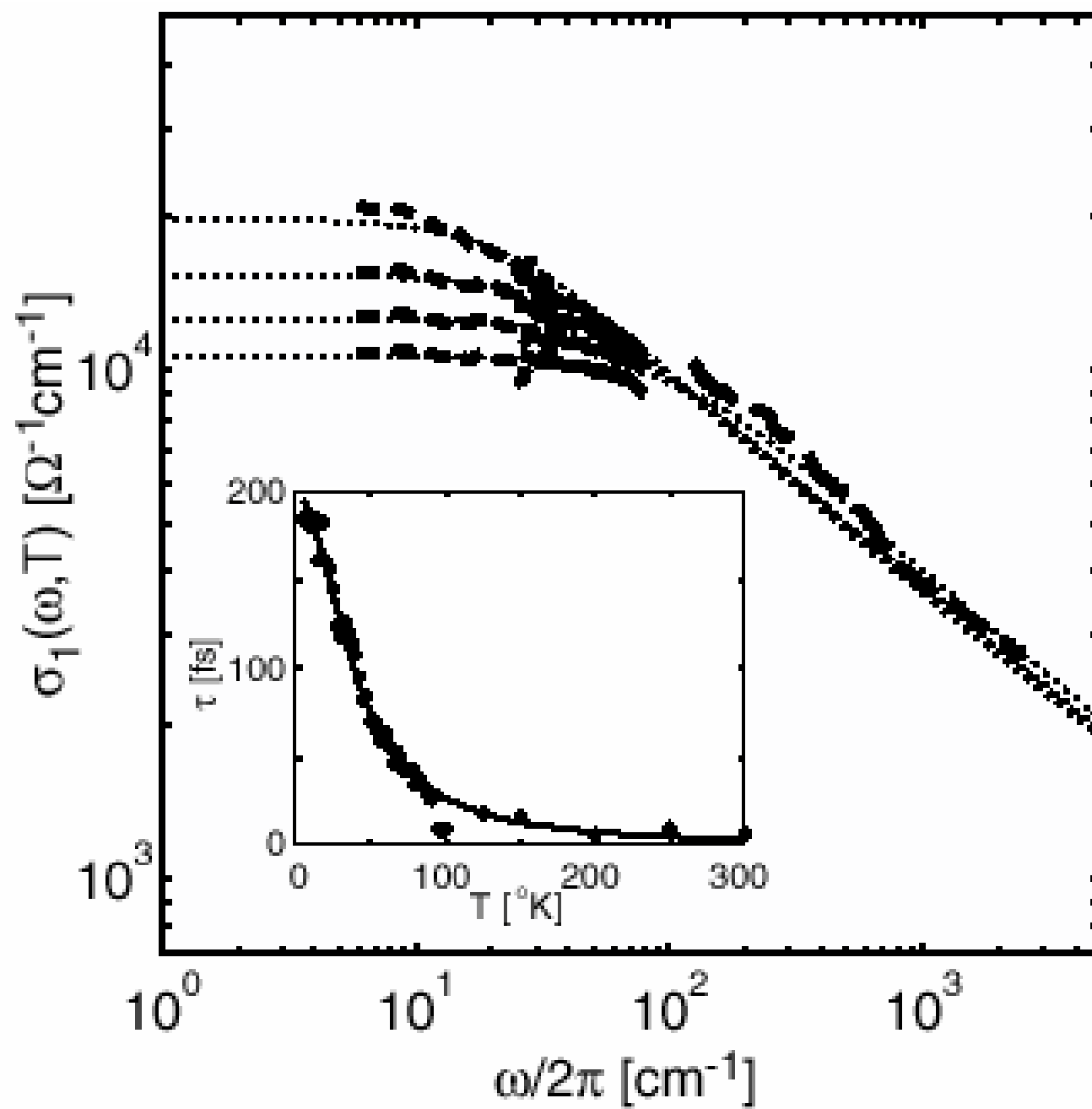


Figure 7

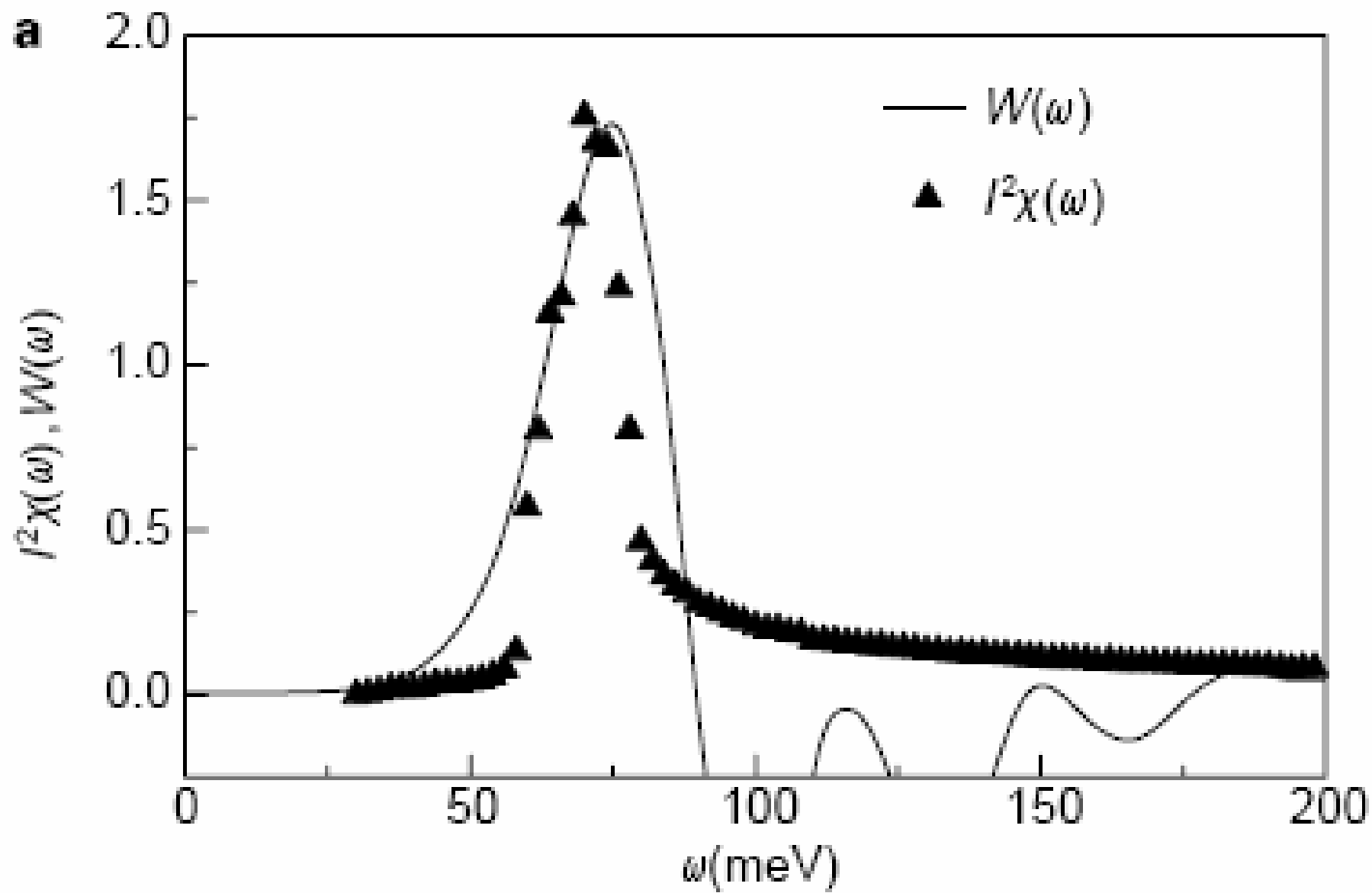


Figure 8

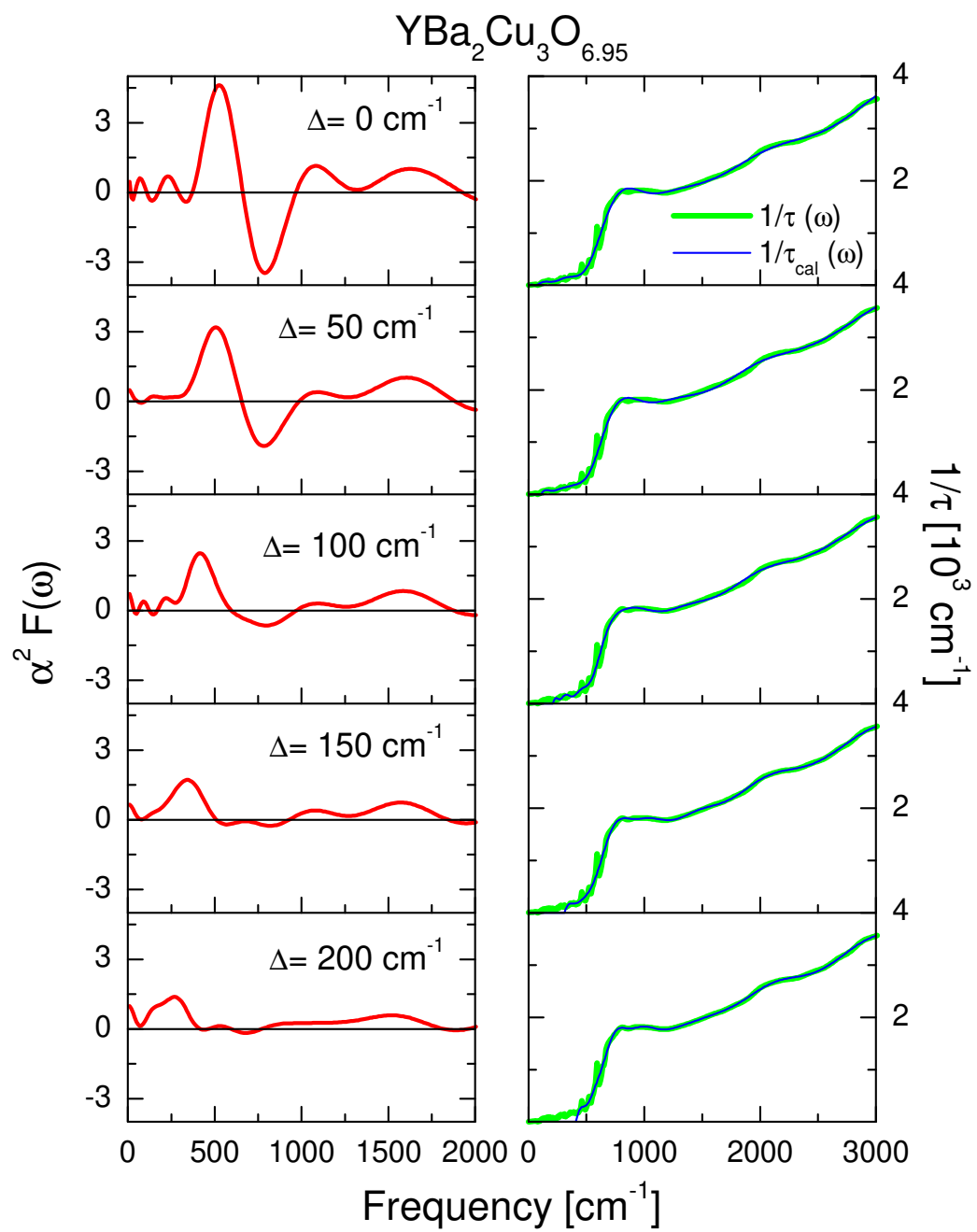


Figure 9

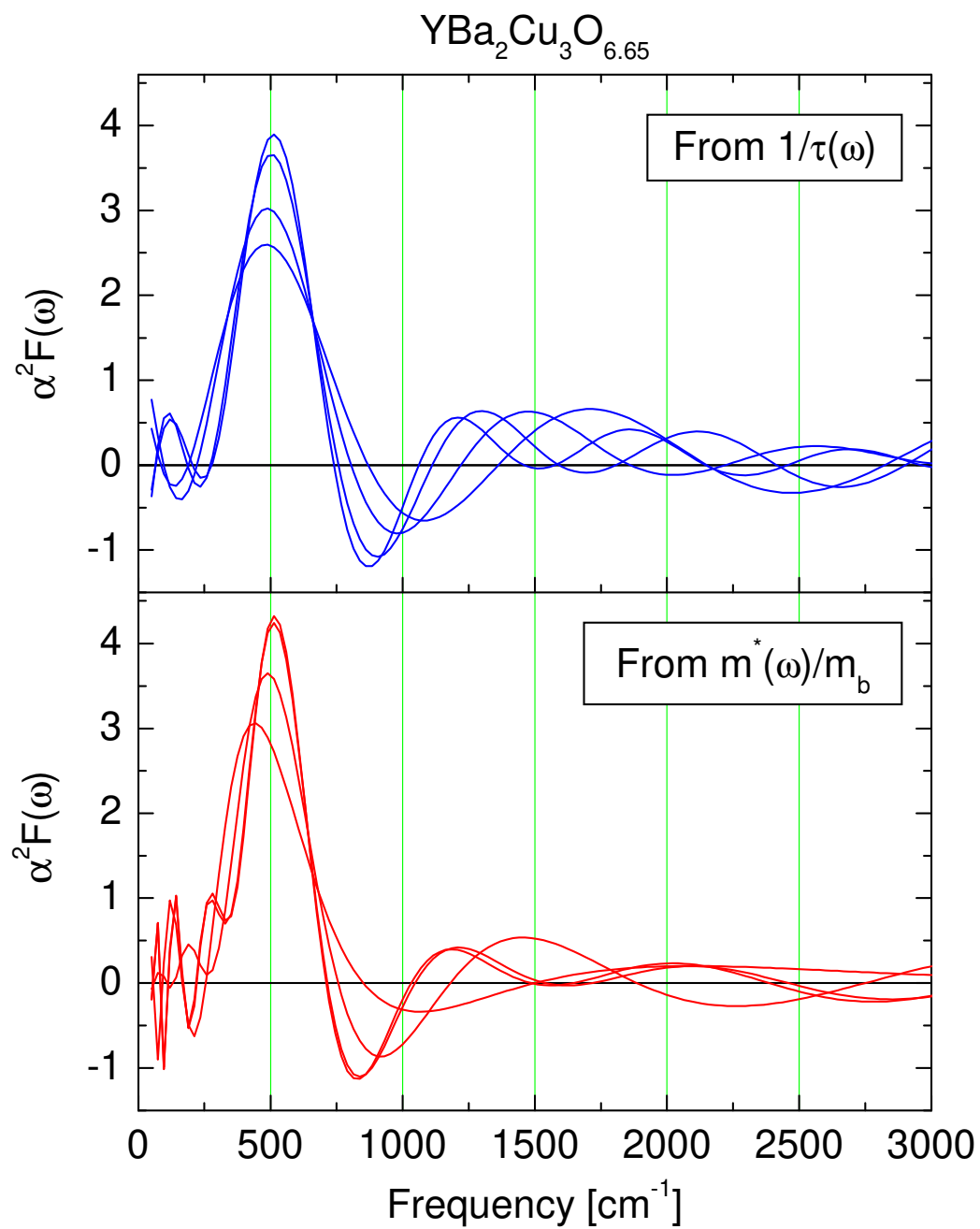


Figure 10

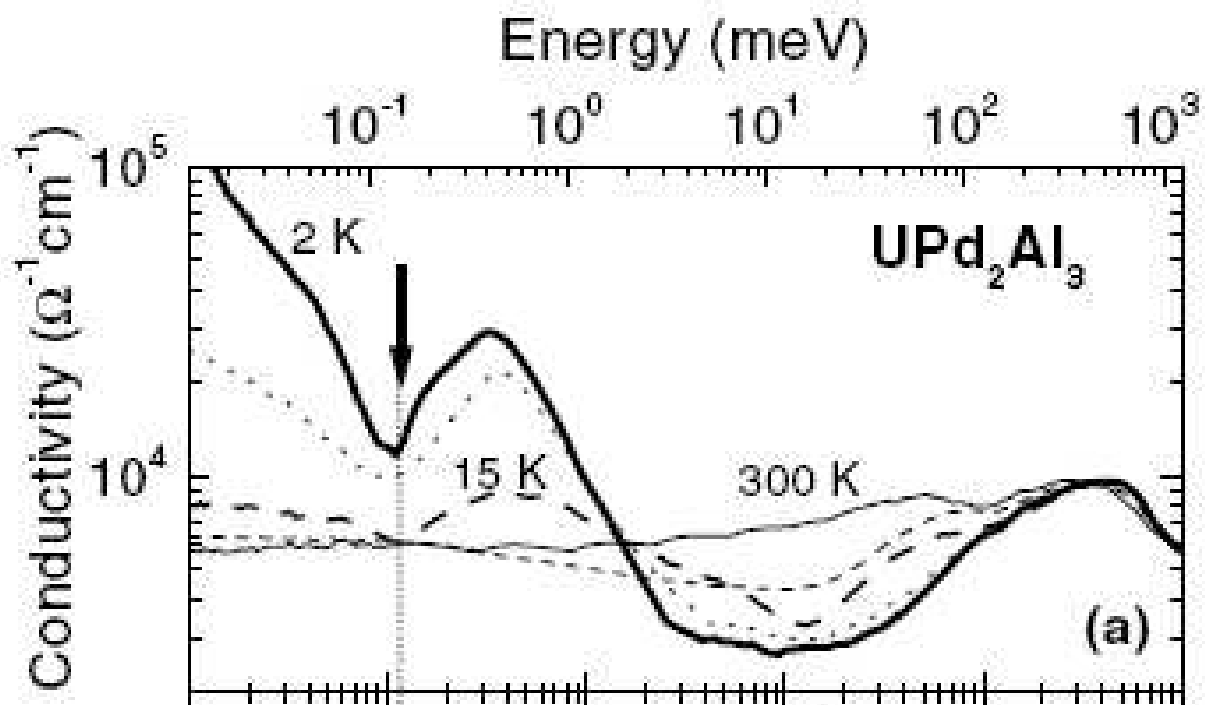


Figure 11

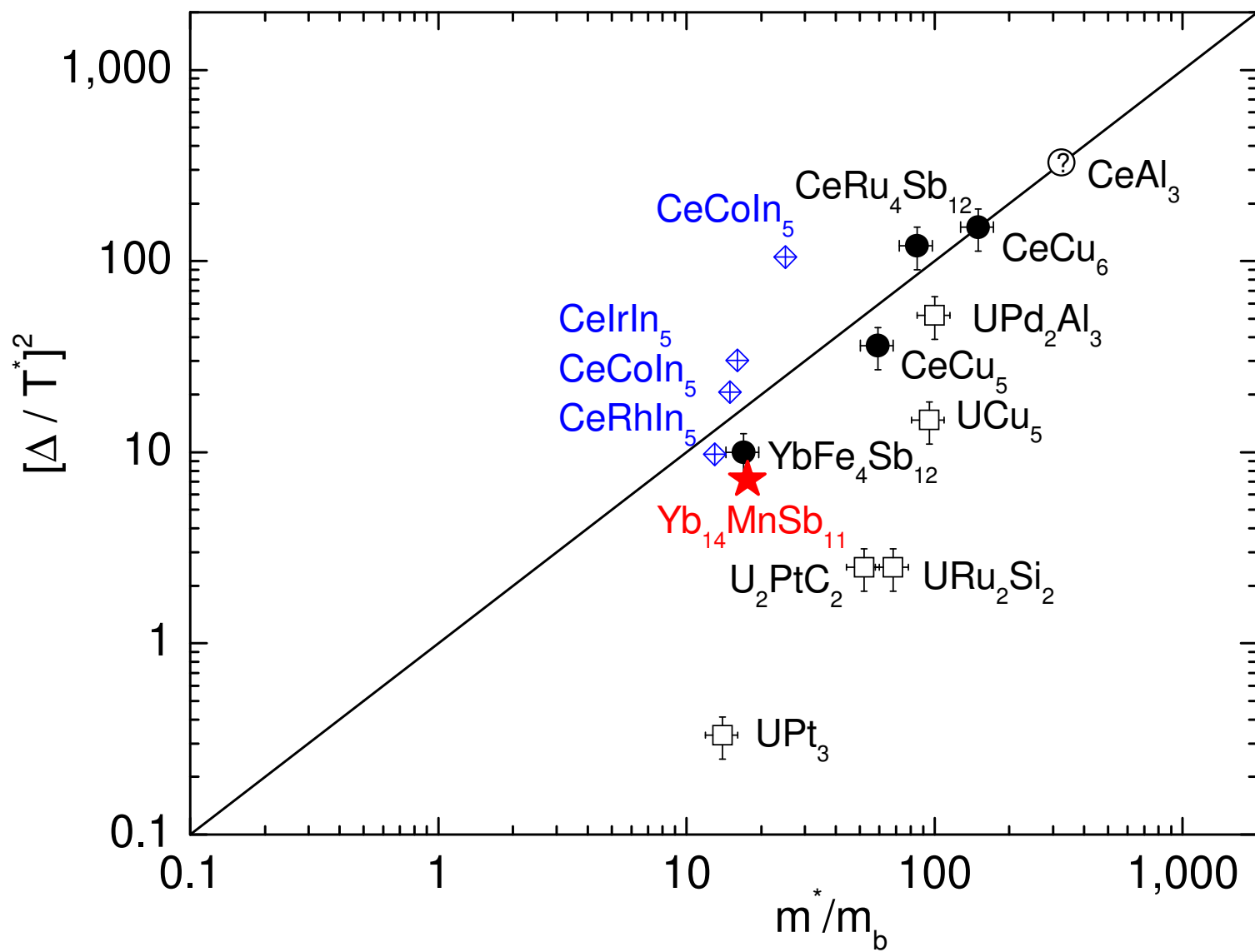


Figure 12

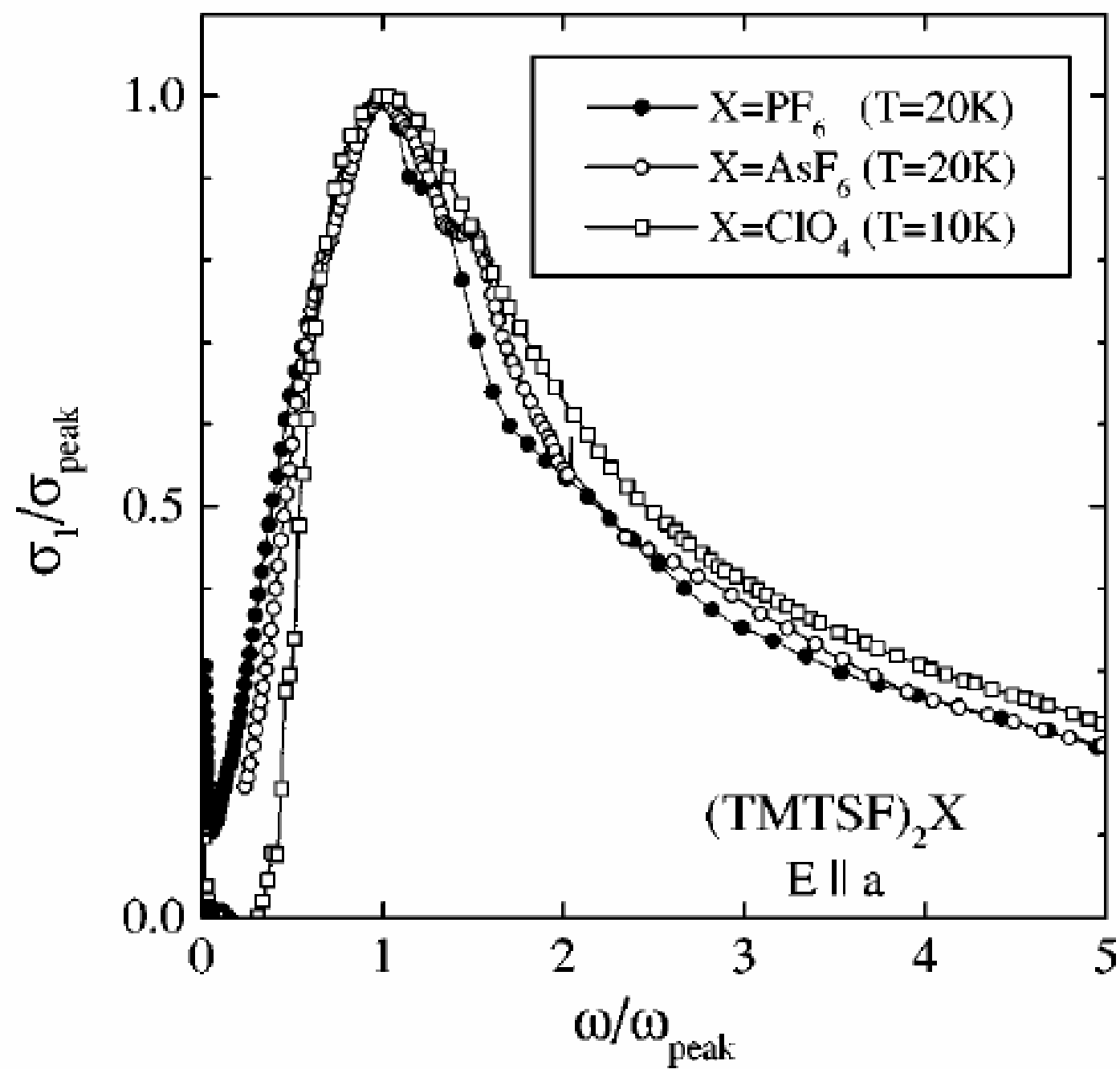


Figure 13

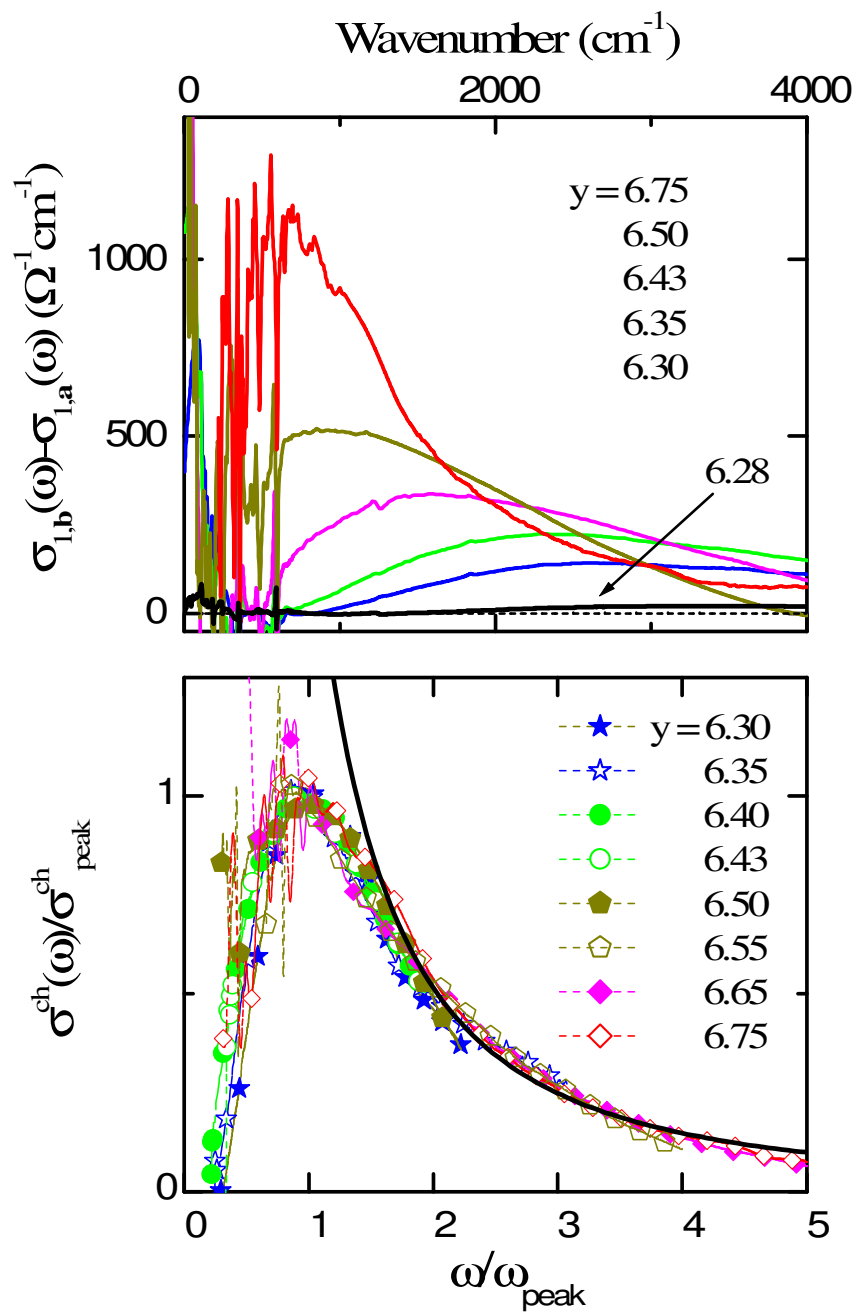


Figure 14

